*minerals*

MDPI

*Article*

# Bismuth Sulfosalts from the Nistru Metallogenetic Field, Baia Mare Zone, NW Romania

**Floarea Damian [1], Gheorghe Damian [2,*], Nigel J. Cook [3], Vsevolod Yu. Prokofiev [4] and Peter András [5]**

[1] Carpathian Association for Environmental and Earth Sciences, Victoriei Street 47A/6, 430142 Baia Mare, Romania; floareadamian@yahoo.com
[2] Department of Geology, Alexandru Ioan Cuza University of Iasi, 20A Carol I Blv., 700505 Iasi, Romania
[3] School of Chemical Engineering, University of Adelaide, Adelaide, SA 5005, Australia; nigel.cook@adelaide.edu.au
[4] Institute of Geology of Ore Deposits, Petrography, Mineralogy, and Geochemistry, Russian Academy of Sciences (IGEM RAS), Sciences, Staromonetny per. 35, Moscow 119117, Russia; vpr@igem.ru
[5] Faculty of Science, Matej Bel University, Tajovského 40, 974 01 Banská Bystrica, Slovakia; peter.andras@umb.sk
* Correspondence: gheorghe.damian@uaic.ro

**Abstract:** An association of bismuth sulfosalts coexisting with native gold is described from a sulfide-rich copper vein in the Nistru area, Baia Mare metallogenetic district, NW Romania. This mineralization is hosted within a Neogene calc-alkaline subvolcanic porphyry quartz-micromonzodiorite stock on the southern border of the Gutâi Mountains. Cu+Au+Bi mineralization represents the inner part of a zoned vein of a type specific to the SE part of the Nistru orefield. The Pb-Zn and Au-Ag veins are located towards the external zone at the boundary of the stock with the surrounding rocks. Bismuth sulfosalts are mainly represented by bismuthinite derivatives and members of the lillianite homologous series. Cosalite, matildite and wittichenite are also present in subordinate amounts. Bi-rich members of the bismuthinite-aikinite series (from krupkaite to bismuthinite) are predominant. A phase with the empirical formula $CuPbBi_7S_{12}$ was also identified and could potentially be a new bismuthinite derivative. The lillianite homologous series is represented by phases with composition between $Gus_{73}$ and $Gus_{59}$, with a dominance of members closer to gustavite ($Gus_{97–79}$) and less abundant members closer to lillianite ($Gus_{49}$). Native gold and Bi-sulfosalts are closely associated with the main sulfides (pyrrhotite, pyrite, chalcopyrite) and quartz, indicating simultaneous crystallization. Fluid inclusion data for quartz indicate a temperature interval between 205 and 247 °C. The assemblage within this vein was deposited from a low-salinity fluid (0.4–2.6 wt.% NaCl equiv.) and density from 0.80 to 0.87 g/cm$^3$.

**Keywords:** sulfides; bismuth sulfosalts; native gold; copper-gold mineralization; Nistru area; Baia Mare metallogenetic district NW Romania



**Citation:** Damian, F.; Damian, G.; Cook, N.J.; Prokofiev, V.Y.; András, P. Bismuth Sulfosalts from the Nistru Metallogenetic Field, Baia Mare Zone, NW Romania. *Minerals* **2024**, *14*, 1182. https://doi.org/10.3390/min14111182

Academic Editor: Georgy Cherkashov

Received: 28 September 2024
Revised: 7 November 2024
Accepted: 17 November 2024
Published: 20 November 2024



## 1. Introduction

Bismuth sulfosalt minerals are described from a broad range of mineralization types and in various paragenetic associations. They have been reported to form at conditions ranging from fumarolic encrustations in volcano craters at temperatures of 500 °C [1], from late-stage of granite-pegmatites [2–7] epithermal-porphyry environments [8], high-sulfidation epithermal [9], low-sulfidation epithermal [10–14], copper skarns [15–22] and related to mineralization hosted within shear zones [23–25]. The structural and chemical characteristics of Bi-sulfosalts are of particular interest and have been extensively researched. Many Bi-sulfosalts form homologous series, groups of closely related minerals that can be classified following a modular structural approach [26–30].

On Romanian territory, the most studied occurrences of Bi-sulfosalts are those in the Apuseni Mts., Poiana Ruscă Mts. and in Southern Banat, where the occurrences are genetically related to skarn systems of Upper Cretaceous age [15,16,31,32].

Cook and Ciobanu [33] described Bi-sulfosalts associated with Bi-tellurides in the younger (Neogene) hydrothermal system at Larga in the Metaliferi Mts. Bi-sulfosalts are, however, relatively minor in the Neogene ores and are usually subordinate to the abundant tellurides.

Cook [12] chemically documented the first occurrence of Bi-sulfosalts associated with the Toroiaga subvolcanic bodies from Baia Borsa within the Neogene metallogenetic province of NW Romania. Cook 1998 [34] described Bi-sulfosalts from hydrothermal vein deposits of Neogene age, N.W. Romania (Băiuț Văratec, Gutâi Mts). Costin and Șerban [35] identified a number of Bi-minerals associated with native gold in Pb-Zn-Cu>Au-Ag ores from the Văratec Baiut ore field. Bismuth sulfosalts without gold have been described from the Cremenea vein, Șuior [36], thus showing that Bi-sulfosalts may occur across the entire Baia Mare metallogenetic district. A new occurrence of Bi-sulfosalts has indeed recently been described from the Baia Sprie ore deposit in the eastern part of the Baia Mare metallogenetic district [10].

Preliminary data addressing the relationship between Bi-sulfosalts and native gold from the Nistru zone, in the southern part of the Gutâi Mts., were reported by Damian [37]. Further accounts of Bi-sulfosalt occurrences from the Nistru and Băiuț areas are given by Plotinskaya et al. [38]; the latter documented the subordinate presence of tetradymite for the first time. An occurrence of Bi-sulfosalts has been reported from deep levels within the similarly aged epithermal Au-(±Cu-Ag-base metal) ore deposit at Beregovo, Transcarpathian Ukraine [39]. We also note the complex association of Bi-sulfosalts related to high-sulfidation epithermal mineralization of Neogene age in the Hodruša mining district, Slovakia [13], as well as an assemblage of Ag–Pb–Bi±Cu sulfosalts from the Bieber vein, Banská Štiavnica deposit [11]. Mineralogical associations of Bi-sulfosalts, tellurides, native gold and jonassonite from the Highiş Massif [24], in skarns [15] and in the Larga-Fața Băii hydrothermal system, Metaliferi Mts., are all suggestive of the role of bismuth melt as a gold scavenger, a mechanism for Au concentration that has been verified by experiment [40]. Ciobanu et al. [41] demonstrated that the structures of some Bi-sulfosalts and tellurides allow the incorporation of lattice-bound gold.

## 2. Geological Setting

The Nistru orefield is located in the southern part of the Gutâi Mts., NW Romania (Figure 1A). The Gutâi Mountains represent the Central Segment of calc-alkaline magmatic activity related to Neogene subduction rollback, collision and extension [42]. According to K-Ar radiometric data, the time interval for volcanic activity in the Gutâi Mts. is 13.4–9.0 Ma [43] or 14–9 Ma [44], extending from the Badenian-Sarmatian boundary to the Upper Pannonian.

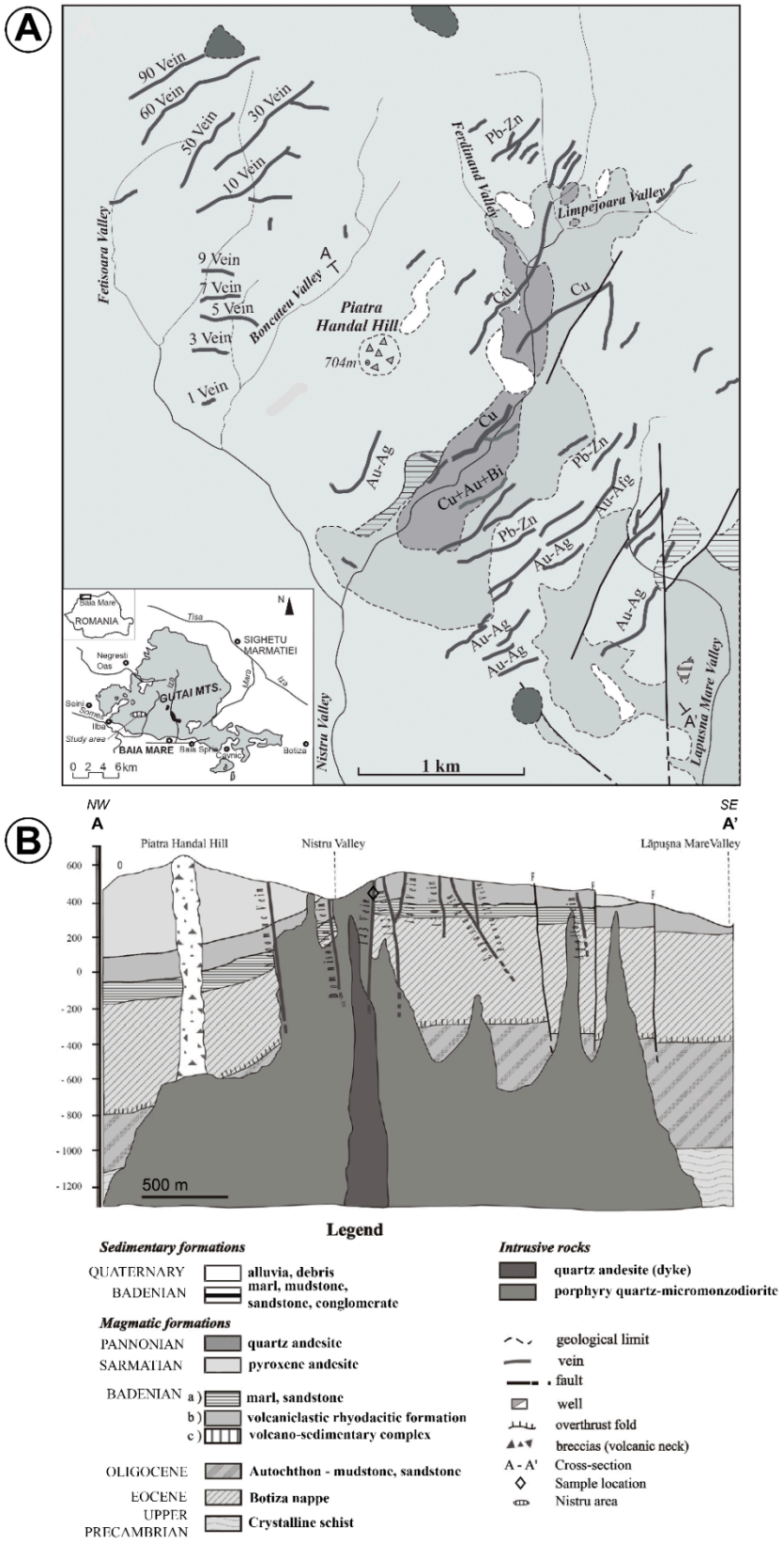


**Figure 1.** (**A**). Geological sketch map of the Nistru area showing the lateral zonation of the ore deposits in the NW–SE orefield. (**B**). Cross-section A–A′ (NW-SE) after Damian et al. [45] and sample location (◊) in the Vein 143 (Lat. 47°33′365″ N./Long. 23°46′5639″ E).

The Nistru area is characterized by extensive development of Sarmatian pyroxene andesites, which are dated as 13.4 to 12.1 Ma [43] and 13.3–12.1 Ma [44], and subordinate Pannonian quartz andesites in the northern and south-eastern parts of the area. The Badenian units are represented by volcaniclastic sequences, mainly pyroclastic flows and volcano-sedimentary rocks [46].

Relationships between igneous rocks, sedimentary units and hydrothermal mineral deposits are presented in Figure 1A,B. The main geological formations are Badenian sedimentary rocks associated with rhyodacitic pyroclastic products (collectively forming the Badenian volcanic-sedimentary complex) and Neogene volcanics (Badenian rhyodacitic pyroclastites, Sarmatian pyroxene andesites and Pannonian quartz andesites). A suite of subvolcanic bodies has been intercepted at depth in the north-western part of the Nistru orefield; they outcrop in the north-eastern part of the Nistru Valley (Figure 1A) over 2.5 km NNE of Piatra Handal Hill. The subvolcanic magmatic bodies post-date the Sarmatian pyroxene andesites sequence. The suite of intrusive magmatic rocks is represented by varieties of porphyritic and subordinate equigranular structures. They differ in their morphological and structural characteristics and petrographic type [45]. K/Ar radiometric data obtained on a porphyry quartz-micromonzodiorite stock sample reveal an age of 10.9 Ma (written comm., Zoltán Pécskay Hungarian Academy of Sciences MTA Institute of Nuclear Research). Neogene basement comprises crystalline rocks belonging to the Middle Dacides and Paleogene formations of Transcarpathian Flysch [47].

## 3. Hydrothermal Mineralization

Hydrothermal ore deposits in the Nistru metallogenetic field are represented by distinct veins systems with base metal and Au-Ag character that correspond to low-sulfidation epithermal type. Lang et al. [48] obtained a time interval for mineralization of the Nistru area: 11.5–10.8 Ma from K/Ar dating; and 10.6 Ma from $^{40}Ar/^{39}Ar$ dating.

The veins are grouped around intrusive bodies. The intrusive bodies are detected up to a depth of 200 m in underground mining levels. Mineralization is deposited within fractures with a vertical zonality that is observed in all veins in the NW part of the Nistru orefield.

The following paragenetic sequence is recognized from depth towards the surface: pyrite-chalcopyrite-quartz-hematite-chlorite; pyrite-chalcopyrite-sphalerite-galena-quartz; pyrite-sphalerite-galena-hematite-marcasite-gold-Ag-sulfosalts-quartz-carbonates. In the SE part of the deposit, a lateral zonation is noted surrounding an apophysis of the subvolcanic porphyry quartz-micromonzodioritic stock, which outcrops on the Nistru Valley [45].

Three ore stages are identified in the SE ore field at Nistru: (1) Cu±Au and Bi; (2) towards the external zone at the boundary of the stock with the surrounding rocks Pb-Zn; and (3) Au-Ag. Copper ores of the first stage are composed of three successive assemblages of (1) pyrite-chalcopyrite-hematite-quartz-sericite; (2) pyrite-chalcopyrite-quartz; and (3) pyrite-chalcopyrite-native gold-Bi-sulfosalts-quartz [37], with the sporadic presence of tetradymite also noted [38]. The later base-metal mineralization is composed of pyrite, chalcopyrite, sphalerite, galena, native gold, tetrahedrite and Pb-As-sulfosalts with calcite and quartz as gangue minerals. The third stage (gold-mineralization) contains an assemblage of pyrite, native gold and Ag-sulfosalts assemblage with kaolinite and halloysite as gangue minerals.

Copper-bearing veins are observed in the central part of the subvolcanic body, whereas Pb-Zn-dominant veins are seen to encircle them (Figure 1A). Gold veins with low sulfide contents occur in the distal areas. Subordinately, at deeper levels within the quartz-micromonzodiorite stock, there are indications for porphyry-style mineralization, characterized by the zonation of hydrothermal alteration types [45].

Bismuth-sulfosalts were identified in the SE part at relatively shallow levels (+526 m) in the "Valea Mare adit", Nistru Valley (Figure 1B). The Cu-Au-Bi association is typical for Vein 143 (Figure 1B), situated on the eastern contact area of the subvolcanic porphyry quartz-micromonzodioritic stock. The porphyry quartz-monzodiorite stock hosting the Cu-Au-Bi vein displays pervasive potassic alteration.

## 4. Materials and Methods

### *4.1. Reflected Light Microscopy*

Samples from the Cu-Au-Bi vein (Figure 1) were examined in reflected light microscopy using a Jenapol polarizing microscope (please provide the manufacture of the instrument, and the address (city, country) of the manufacture). Interest in this mineralization is due to the high concentration of Au, which is up to 43 g/t, as well as Ag up to 93 g/t, as revealed by chemical analysis. An abundance of native gold grains associated with bismuth minerals and sulfides was evident from the microscopic study in reflected light.

### *4.2. Electron Probe Microanalysis*

Chemical compositions were determined using electron probe microanalysers at IGEM-RAS (Moscow) and the State Geological Institute of Dionyz Stur (Bratislava, Slovakia). At IGEM-RAS, analyses were made using a JEOL JCXA 8100 SUPERPROBE) (JEOL, Tokio, Japan) equipped with a WDX-detector, operated at a 20 KV accelerating voltage, 20 nA sample current and a beam diameter of 1–2 μm. Count times were from 10 to 20 s. The following peaks were measured: Kα (for Cu, S, Fe and Zn), Lα (for Te, Ag, Sb, As, and Se) and Mα (for Bi, Pb, Hg, and Au). PbS, CdSe, Bi2Te3, CuFeS2, Ag3SbS3, As2S3, HgS, $Sb_2S_3$, ZnS and pure Au were used as standards. A ZAF correction was used to avoid peak overlap.

Analyses performed in Bratislava were made on a Cameca SX-100 Electron Probe Microanalyzer (CAMECA, Gennevilies Cedex, France) on carbon-coated polished sections. Measurements were performed using a 25 kV acceleration voltage, 15–20 nA beam current, 5 μm beam diameter, 20 s peak count times and 7 s for the background. The following X-ray lines and natural (n) or synthetic (s) standards were used: S Kα (n-$CuFeS_2$), Fe Kα (n-$CuFeS_2$), Pb Mα (n-PbS), Cu Kα (n-$CuFeS_2$), Sb Lβ (n-$Sb_2S_3$), Se Lβ (s-$Bi_2Se_3$), Te Lα ($Bi_2Te_3$) and pure metals for Ag Lα and Bi Lα. Typical minimum detection limits were 0.02 wt.% for Ag and Se, 0.03 wt.% for Fe, Cu, Sb and Te, 0.05 wt.% for S, 0.07 wt.% for Bi and 0.16 wt.% for Pb.

### *4.3. Fluid Inclusion Microthermometry*

Microthermometric analysis of the individual fluid inclusions was carried out using a Linkam THMSG 600 heating/freezing stage (Linkam Scientific Instruments Ltd., Redhil, UK in combination with an Olympus BX51 optical microscope–Olympous Corp., Tokyo, Japan) and digital video camera at the Institute of Geology of Ore Deposits, Mineralogy, Geochemistry and Petrography, Russian Academy of Sciences, Moscow. This method enables an estimation of the chemical composition of the fluid trapped in the inclusions from the temperature of phase transition and transformation at heating and freezing. Between −20 and +20 °C, the uncertainty of measurements is ±0.2 °C and decreases at higher and lower temperatures. The composition of salts predominant in aqueous solutions that fill the inclusions was estimated at eutectic temperature [49]. The total concentration of salts in two-phase inclusions of the second type was estimated from ice melting temperature according to the experimental data on the NaCl–$H_2O$ system [50]. The partial pressure of $CO_2$ was determined for immiscible fluids from the intersection of isochore and isotherm [51]. The salinity, density and pressure of the fluid were calculated with the FLINCOR program [52].

Bulk inclusion analysis using gas chromatography, ion chromatography and ICP-MS was carried out according to the techniques reported by Kryazhev et al. [53] at the Central Institute of Geological Exploration for Base and Precious Metals, Moscow. The analyzed samples were 0.5 g aliquots of milled quartz (0.25 to 0.5 mm sieved fractions). Water content was determined by gas chromatography to calculate the concentration of elements in the hydrothermal solution. Concentrations of $CO_2$ and $CH_4$ were also determined. The contents of Cl, K, Na, Ca, Mg and other elements were measured utilizing ICP-MS methods.

## 5. Results

### *5.1. Mineral Assemblages*

Pyrite is the dominant sulfide mineral and forms parallel or irregular massive aggregates in the marginal part of grey quartz veins. Pyrite crystals range from euhedral to subhedral (Figure 2a–d). Some pyrite crystals from the central area of the vein are incipiently dissolved (Figure 2e), while some from the marginal area are slightly rounded towards boundaries with chalcopyrite. Pyrite plays an important role as a host mineral for microscopic inclusions of native gold in Vein 143 (Figures 1B and 2b,c). The presence of "invisible gold" with an average concentration of 33.4 ppm was also determined via secondary-ion mass spectrometry on nine pyrite grains with an average As concentration of 1.1 wt.%. Pyrite is frequently associated with arsenopyrite, which occurs as euhedral rhomb-shaped or anhedral crystals.

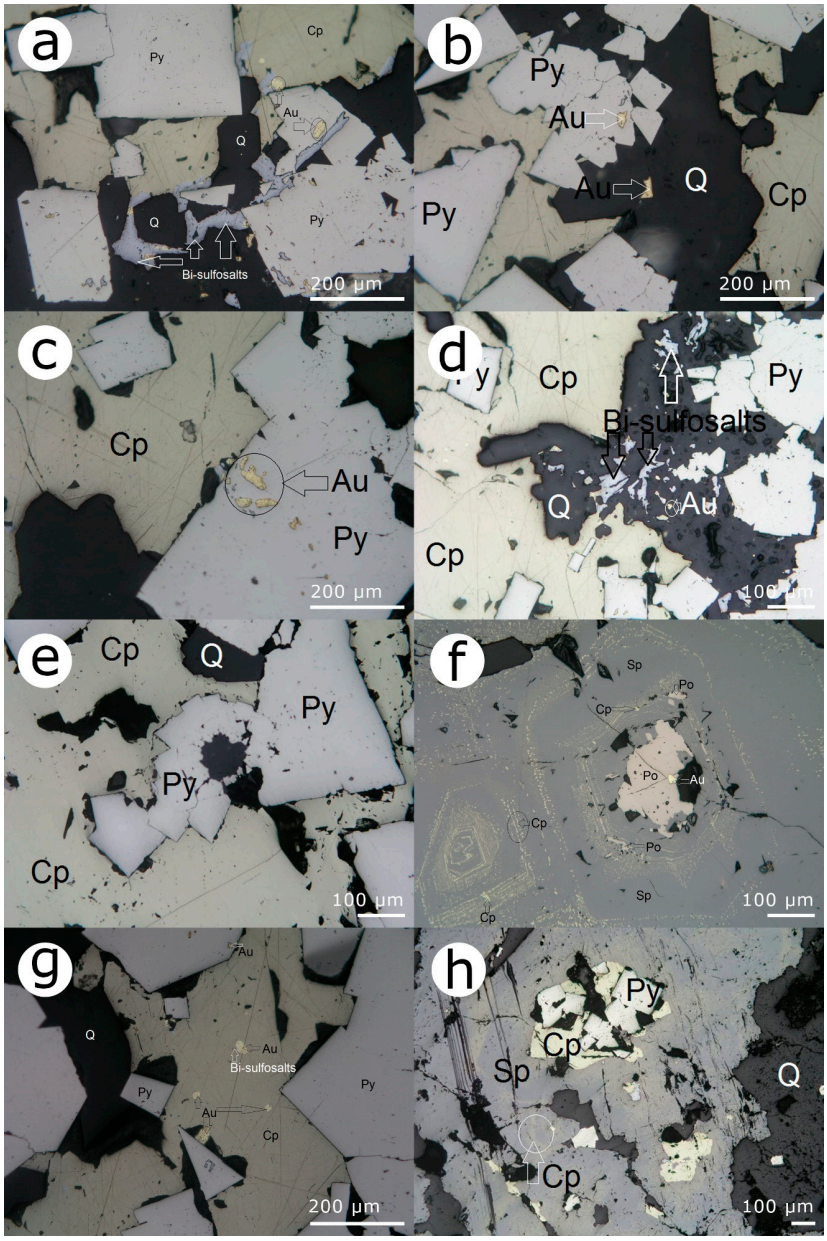


**Figure 2.** Photomicrographs in reflected light showing textural aspects of the assemblage containing native gold and Bi-sulfosalts. (**a**) Native gold—Bi-sulfosalts—sulfides assemblage. (**b**) Native gold

inclusion in pyrite and in euhedral quartz. (**c**) Native gold inclusion in pyrite. (**d**) Pyrite associated with chalcopyrite and Bi-sulfosalts within quartz. (**e**) Radiating aggregates and euhedral crystals of pyrite inclusion in chalcopyrite. (**f**) Pyrrhotite as a small crystal associated with the native gold on growth surfaces within sphalerite, sphalerite contains exsolutions of chalcopyrite and of pyrrhotite. (**g**) Chalcopyrite with inclusions of native gold and Bi-sulfosalts, quartz pyrite. (**h**) Sphalerite as coarse aggregates with abundant chalcopyrite exsolutions, containing euhedral crystals of pyrite and chalcopyrite. Abbreviations: Au—native gold; Cp—chalcopyrite; Py—pyrite; Po—Pyrrhotite; Q—quartz.

Pyrrhotite appears as small crystals associated with the native gold and as exsolutions within sphalerite (Figure 2f).

Chalcopyrite is the dominant sulfide in the central area of Vein 143 (Cu+Bi+Au, Figure 1B). Chalcopyrite contains inclusions of native gold, Bi-sulfosalts and euhedral sphalerite (Figure 2f).

Sphalerite occurs as xenomorphic aggregates containing chalcopyrite as micron-sized exsolutions, randomly dispersed or aligned in rows along crystallographic planes (Figure 2f,h). Rarely, sphalerite contains inclusions of pyrrhotite (Figure 2f). Sphalerite from the assemblage with pyrrhotite contains a higher FeS component (up to 21 mol.% FeS) relative to the assemblage with pyrite (up to 17.8 mol.% FeS) [54]. The formation temperature for this association is >300 °C, according to Plotinskaya et al. [54].

Native gold occurs commonly as rounded grains in the quartz matrix or included within idiomorphic pyrite or chalcopyrite and rarely in pyrrhotite (Figure 2a–c). The native gold grains are frequently associated with the Bi-minerals (Figure 2a). The gold association with the Bi-minerals and their relationships with pyrite, chalcopyrite and quartz suggests simultaneous precipitations. Native gold within copper mineralization containing Bi-sulfosalts has a relatively low Ag content, rangeing from 20.46 to 23.35 wt.% [38].

### *5.2. Bismuth Minerals*

Compositions of Bi-minerals were documented by EPMA. They occur as bismuthinite derivatives and phases of the lillianite homologous series. Other Bi-sulfosalts were identified in subordinate amounts, cosalite, matildite and wittichenite, in order of abundance. Bismuth sulfosalts are observed in the following associations:

(i) As inclusions in coarse chalcopyrite that cements grains of corroded pyrite (Figure 3a).
(ii) Along the marginal areas of coarse chalcopyrite at the margin adjoining quartz from the vein matrix, associated with isometric native gold (Figure 3b,e).
(iii) As anhedral crystals, associated with the gold and chalcopyrite that are included in the quartz matrix (Figure 3c).
(iv) Commonly, as grains dispersed in the quartz vein matrix.
(v) As aggregates in which bismuthinite derivatives and lillianite homologs occur either alone or intergrown with one another (Figure 3d,f).
(vi) Lillianite-gustavite crystals with matildite inclusions are associated with bismuthine lamellae (Figure 4b,c).
(vii) Lamellar to granular crystals of lillianite-gustavite included in chalcopyrite are rimmed by a thin film of wittichenite (Figure 3c).
(viii) Occurs sporadically as inclusions in chalcopyrite (Figure 3f).

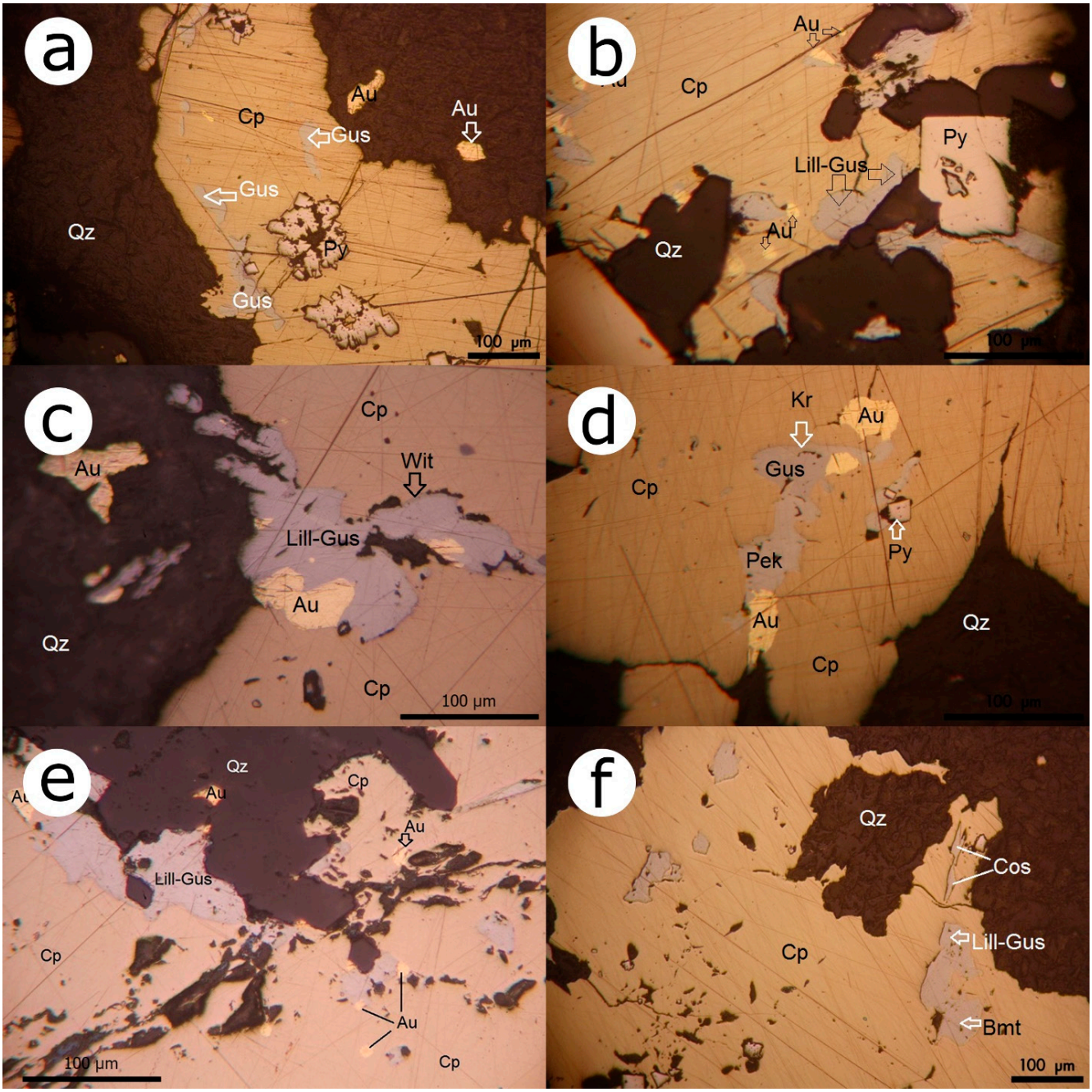


**Figure 3.** Reflected light microphotographs showing the occurrence of Bi-minerals with native gold: (**a**) Bi-sulfosalts within compact masses of chalcopyrite that cemented dissolved pyrite crystals. (**b**) Bi-sulfosalts lillianite-gustavite and native gold located at boundaries between quartz and chalcopyrite. (**c**) Bi-sulfosalts: lillianite-gustavite, wittichenite associated with native gold and chalcopyrite within the quartz matrix. (**d**) Intergrown of the krupkaite and pekoite with lillianite-gustavite with native gold included in chalcopyrite. (**e**) Bi-sulfosalts (lillianite-gustavite) and native gold within chalcopyrite and in the contact zone with quartz. (**f**) Cosalite, lillianite-gustavite and bismuthinite enclosed in chalcopyrite in the quartz matrix. Abbreviations: Au—native gold, Cp—chalcopyrite; Py—pyrite; Lill-Gu—lillianite-gustavite; Wit—wittichenite; Kr—krupkaite; Pek—pekoite; Cos—Cosalite; Bmt—bismuthinite; Qz—quartz.

Textural relationships between sulfides and Bi-sulfosalts minerals in association with native gold indicate two main paragenetic sequences: (1) an early sequence in which pyrite, arsenopyrite and pyrrhotite, followed by chalcopyrite and sphalerite, were deposited;

and (2) a late sequence when the bismuth minerals and the majority of the native gold was deposited. The existence of the two stages is supported by petrographic evidence showing the dilution and corrosion of the pyrite crystals (Figure 2e). The central parts of the Cu+Bi+Au vein contain compact quartz crossed by bands of milky white quartz with bismuth minerals and native gold. The bismuth compounds of the two sequences have crystallized simultaneously with cosalite and are followed by wittichenite. The two mineralization sequences could be related to the sequential layout of the subvolcanic bodies from the Nistru area [45].

#### 5.2.1. Bismuthinite-Aikinite Series

EPMA data for bismuthinite derivatives ($Bi_4S_6$-$Cu_2Pb_2Bi_2S_6$) are given in Table 1. The series contains intermediate members between bismuthinite and aikinite [55], including several more recently discovered minerals (salzburgite, paarite and emilite [56].

**Table 1.** Representative electron microprobe analyses of bismuthinite derivatives in the Nistru, Baia Mare area.

| Number | Weight% | | | | | | | | | | Mineral |
|---|---|---|---|---|---|---|---|---|---|---|---|
| | Bi | Pb | Te | Sb | Ag | Cu | Fe | Se | S | Total | |
| NV8 Bi-1 | 75.68 | 3.91 | 0.02 | 0.05 | 0.01 | 1.68 | 0.18 | 0.09 | 17.94 | 99.57 | close to bismuthinite |
| NV8 Bi-2 | 76.64 | 2.78 | 0.01 | 0.04 | 0.03 | 1.27 | 0.12 | 0.09 | 18.84 | 99.81 | bismuthinite |
| NV8 Bi-3 | 69.81 | 6.53 | 0.04 | 0.04 | 0.00 | 3.18 | 0.65 | 0.15 | 18.63 | 99.01 | close to $CuPbBi_7S_{12}$ |
| Nistru 1D | 71.19 | 8.95 | 0.00 | 0.00 | 0.00 | 2.11 | 0.29 | 0.13 | 18.57 | 101.24 | pekoite |
| Nistru 2D | 74.65 | 4.17 | 0.00 | 0.00 | 0.00 | 1.69 | 0.16 | 0.15 | 18.77 | 99.59 | close to bismuthinite |
| Nistru 3D | 77.51 | 2.93 | 0.09 | 0.00 | 0.00 | 1.88 | 0.64 | 0.26 | 18.71 | 102.02 | close to bismutine |
| Nistru 4D | 74.89 | 4.09 | 0.00 | 0.00 | 0.00 | 2.04 | 0.92 | 0.34 | 18.10 | 100.38 | pekoite |
| Nistru 5D | 66.64 | 12.02 | 0.00 | 0.09 | 0.00 | 3.95 | 0.35 | 0.12 | 17.77 | 100.94 | gladite |
| Nistru 6D | 55.09 | 19.13 | 0.10 | 0.10 | 0.00 | 5.51 | 0.22 | 0.17 | 17.17 | 97.49 | krupkaite |
| Nistru 7D | 55.85 | 18.88 | 0.00 | 0.11 | 0.00 | 6.37 | 0.68 | 0.00 | 17.76 | 99.65 | krupkaite |
| Nistru 8D | 55.82 | 18.39 | 0.00 | 0.00 | 0.00 | 6.35 | 0.70 | 0.17 | 17.74 | 99.17 | krupkaite |
| Nistru 9D | 57.18 | 17.43 | 0.00 | 0.11 | 0.00 | 5.41 | 0.33 | 0.11 | 17.69 | 98.26 | krupkaite |
| 196/2 | 76.29 | 2.18 | 0.06 | 0.00 | 0.24 | 1.97 | 0.85 | 0.09 | 19.13 | 100.82 | pekoite |
| N-1/3 | 78.53 | 1.11 | 0.06 | 0.13 | 0.09 | 0.43 | 0.03 | 0.16 | 18.90 | 99.45 | bismuthinite |
| NV-9/2 | 56.82 | 18.67 | 0.00 | 0.08 | 0.01 | 6.33 | 0.54 | 0.05 | 17.89 | 100.39 | krupkaite |
| NV-9/3 | 56.47 | 18.12 | 0.00 | 0.09 | 0.00 | 6.10 | 0.81 | 0.00 | 18.25 | 99.84 | krupkaite |
| **Chemical Formula on the Basis of 8 Cations.** | | | | | | | | | | | |
| **Number** | **Bi** | **Pb** | **Te** | **Sb** | **Ag** | **Cu** | **Fe** | **Se** | **S** | **naikinite** | |
| NV8 Bi-1 | 7.45 | 0.39 | 0.00 | 0.01 | 0.00 | 0.54 | 0.07 | 0.02 | 11.51 | 12.63 | close to bismuthinite |
| NV8 Bi-2 | 7.40 | 0.27 | 0.00 | 0.01 | 0.01 | 0.40 | 0.04 | 0.02 | 11.85 | 9.40 | bismuthinite |
| NV8 Bi-3 | 6.61 | 0.62 | 0.01 | 0.01 | 0.00 | 0.99 | 0.23 | 0.04 | 11.50 | 24.42 | close to $CuPbBi_7S_{12}$ |
| Nistru 1D | 6.79 | 0.86 | 0.00 | 0.00 | 0.00 | 0.66 | 0.10 | 0.03 | 11.55 | 21.38 | pekoite |

**Table 1.** *Cont.*

| Number | Weight% | | | | | | | | | | Mineral |
|---|---|---|---|---|---|---|---|---|---|---|---|
| | Bi | Pb | Te | Sb | Ag | Cu | Fe | Se | S | Total | |
| Nistru 2D | 7.19 | 0.41 | 0.00 | 0.00 | 0.00 | 0.54 | 0.06 | 0.04 | 11.78 | 12.98 | close to bismuthinite |
| Nistru 3D | 7.32 | 0.28 | 0.01 | 0.00 | 0.00 | 0.58 | 0.23 | 0.07 | 11.51 | 13.82 | close to bismutine |
| Nistru 4D | 7.20 | 0.40 | 0.00 | 0.00 | 0.00 | 0.65 | 0.33 | 0.09 | 11.34 | 17.40 | pekoite |
| Nistru 5D | 6.37 | 1.16 | 0.00 | 0.02 | 0.00 | 1.24 | 0.13 | 0.03 | 11.06 | 33.02 | gladite |
| Nistru 6D | 5.35 | 1.87 | 0.02 | 0.02 | 0.00 | 1.76 | 0.08 | 0.04 | 10.86 | 51.29 | krupkaite |
| Nistru 7D | 5.21 | 1.78 | 0.00 | 0.02 | 0.00 | 1.95 | 0.24 | 0.00 | 10.80 | 55.02 | krupkaite |
| Nistru 8D | 5.22 | 1.73 | 0.00 | 0.00 | 0.00 | 1.95 | 0.25 | 0.04 | 10.81 | 54.72 | krupkaite |
| Nistru 9D | 5.46 | 1.68 | 0.00 | 0.02 | 0.00 | 1.70 | 0.12 | 0.03 | 11.01 | 48.37 | krupkaite |
| 196/2 | 7.14 | 0.21 | 0.01 | 0.00 | 0.04 | 0.61 | 0.30 | 0.02 | 11.67 | 15.47 | pekoite |
| N-1/3 | 7.65 | 0.11 | 0.01 | 0.02 | 0.02 | 0.14 | 0.01 | 0.04 | 12.00 | 3.77 | bismuthinite |
| NV-9/2 | 5.28 | 1.75 | 0.00 | 0.01 | 0.00 | 1.93 | 0.19 | 0.01 | 10.83 | 53.58 | krupkaite |
| NV-9/3 | 5.21 | 1.69 | 0.00 | 0.01 | 0.00 | 1.85 | 0.28 | 0.00 | 10.97 | 53.52 | krupkaite |

Anhedral crystals of bismuthinite derivatives, with sizes between 0.05 and 0.1 mm, are most frequently observed as inclusions within coarse chalcopyrite that have been intensely corroded by quartz. Members of the bismuthinite-aikinite series are found in grain contact with those of the lillianite series (Figure 4a), contrasting with the observations of Cook [34].

Compared to data provided by Cook [34], members of the bismuthinite-aikinite series from the Nistru zone correspond to the same compositional range seen at Baiut in the eastern part of the Baia Mare district in Romania. Bismuth derivatives from Nistru have $n_{aik}$ values between 3.77 and 55.02 (Table 1). The bismuth contents are between 55.09 and 75.678% Bi with the low values assigned to krupkaite and the high values being close to bismuthinite. Tellurium, Se, Sb and Fe are noted in minor amounts within most analyses. Partial substitution of S by Se appears to be a consistent feature of all analyses of bismuth derivatives.

Calculation of formulae for bismuthinite derivatives was performed based on the substitution Cu + Pb → □ + Bi (where □ is the vacant tetrahedral position) and the empirical formula $Cu_xPb_yBi_{8-1/2(x+y)}S_{12}$, on the basis of (1/2 (Cu + Pb) + Bi = 8 atoms per formula unit after Makovicky and Mackovicky [55].

Within the bismuthinite-aikinite series from the Nistru zone (Baia Mare area) $n_{aik}$ (Table 1) represents the percentage of the aikinite members according to Makovicky and Makovicky [55]. Compositions of bismuthinite derivatives are graphically represented in the Bi-Cu-Pb ternary diagram (Figure 5).

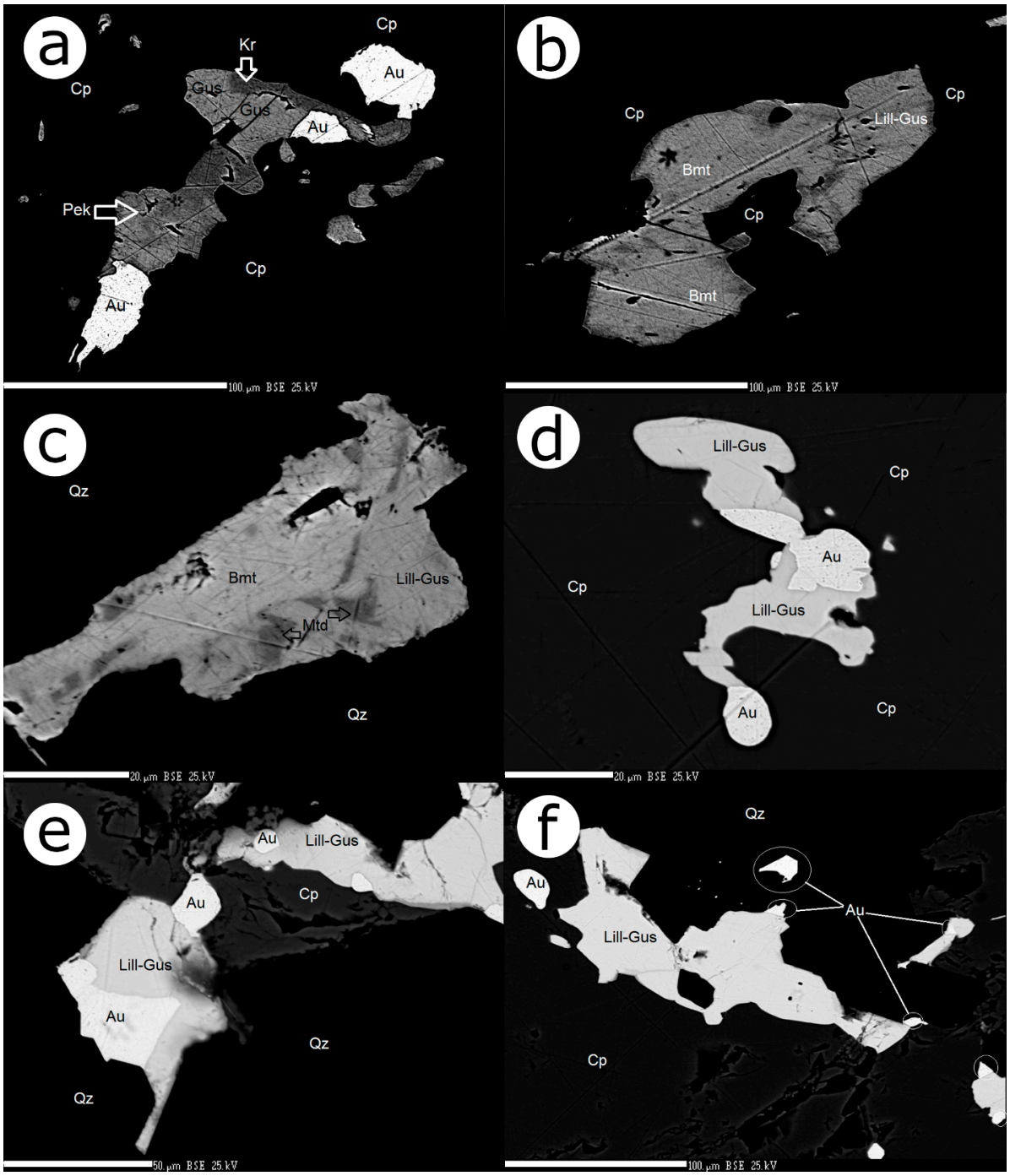


**Figure 4.** Back-scattered electron images of the probe showing paragenetic aspects of Bi-sulfosalt occurrences. (**a**) Native gold associated with lillianite-gustavite intergrowths with krupkaite and pekoite within anhedral chalcopyrite. (**b**) Heterogeneous intergrowths between lillianite-gustavite and bismuthinite in chalcopyrite. (**c**) Lillianite-gustavite is present within lath-shaped grains, with compositional variation specific for matildite and bismuthinite in a matrix of quartz. (**d**) Lillianite gustavite associated with native gold in chalcopyrite. (**e**) Lillianite-Gustavite, native gold and chalcopyrite in a matrix of idiomorphic quartz. (**f**) Lillianite-gustavite and native gold in the marginal zone of chalcopyrite in contact with quartz. Abbreviations: Au–native gold, Cp–chalcopyrite, Lill-Gus–lillianite-gustavite, Kr–krupkaite, Pek–pekoite, Bmt–bismuthinite, Mtd–matildite, Qz–quartz.

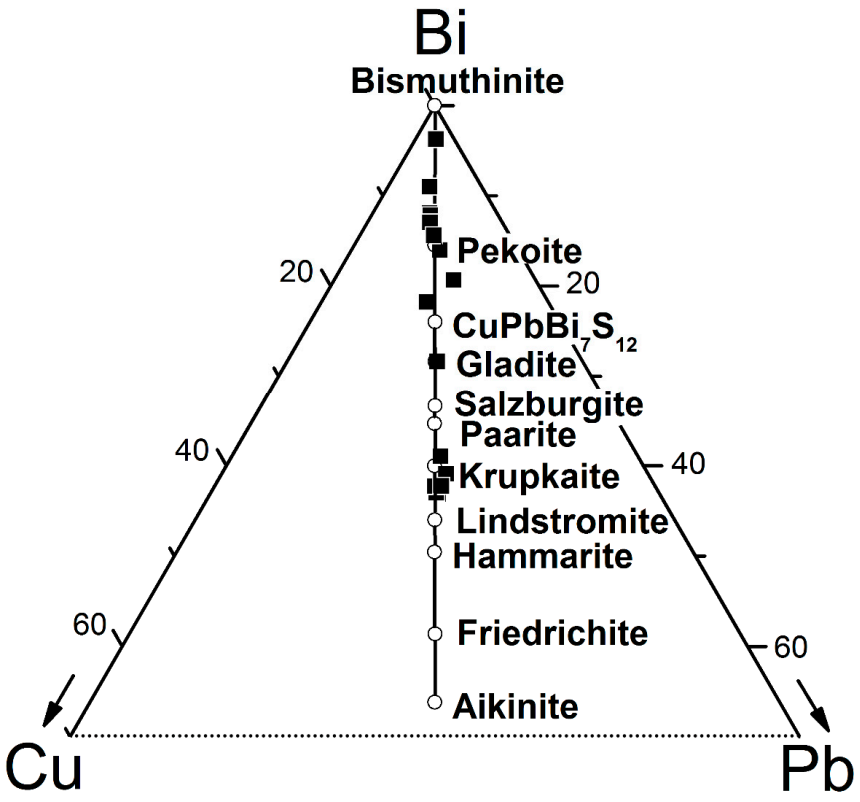


**Figure 5.** Compositional data for bismuthinite derivatives plotted on a Cu-Pb-Bi ternary diagram (atom %).

Analyzed grains all plot on the Bi-rich side of the series, between bismuthinite and krupkaite. Individual analyses cluster around ideal pekoite, gladite and krupkaite compositions, as well as intermediate between these species.

According to their calculated $n_{aik}$ values, bismuthinite derivatives from Nistru are represented by the following: (i) Krupkaite, compositionally halfway between bismuthinite and aikinite, [57]. For krupkaite the value of $n_{aik}$ is between 48.37 and 55.02, comparable with those published by Topa et al. [58]. The extreme values of $n_{aik}$ for krupkaite are correlated to different stages of Pb+Cu substitution for Bi, and correspond to "under-substituted" krupkaite and with "over-substituted" krupkaite, influenced by the interatomic distances [59]; (ii) Members with compositions between bismuthinite and pekoite ($n_{aik}$ = 12.63–13.82), which do not correspond to a known member of the series, according to Topa et al. [58]. There are two sequences of ideal bismuthinite with $n_{aik}$ = 3.77–9.40; (iii) Subordinate pekoite ($n_{aik}$ = between 17.40 and 21.38) and gladite ($n_{aik}$ = 33.02); (v) An unnamed phase of the bismuthinite-aikinite series (sample NV8 Bi-3 Table 1) with $n_{aik}$ = 24.42, corresponding to the empirical formula $CuPbBi_7S_{12}$. This may be analogous to the as-yet-unnamed phase with a similar composition noted elsewhere [6,7,15,23,25]. The members of the bismuthinite-aikinite from Nistru differ from those of Baia Sprie, which correspond to a composition between bismuthine and pekoite [10].

5.2.2. Lillianite-Gustavite Homologous Series

The lillianite homeotypic series $^4$L [30] in the studied mineralization is represented by Bi-rich members, lillianite-gustavite. The level of substitution specific to the lillianite-gustavite series (2Pb ↔ Ag+Bi) after Makovicky and Karup-Møller [29] for the analyzed samples from the Nistru area determines the point disposition along line N = 4. All analyses correspond to members of the lillianite-gustavite solid solution and have chemical *N* values between 3.72 and 4.17 (Table 2). A single analysis revealed a much lower N value (3.56) and plotted away from the lillianite-gustavite line towards galenobismutite. Two other

analyses had somewhat higher N (4.26 and 4.39) and also plotted a little astray from the N = 4 line, even if they are best considered as gustavite. Members of the series from the Nistru area can best be described as the end-member gustavite. The "L" value of the lillianite-gustavite series (Table 2) represents the substitution percentage of Pb by Ag and Bi calculated after Makovicky and Karup-Møller [28]. The composition extends into the proposed immiscibility zone between $Gu_{50}$ and $Gu_{85}$ under natural hydrothermal conditions [28,30]. Such compositions compare closely to those described by Cook [12,34] from the Baia Borșa and Baiuț-Văratec areas, as well as those reported by Buzatu et al. [10] from the Baia Sprie area, Baia Mare district.

**Table 2.** Representative electron microprobe analyses of lillianite-gustavite in the Nistru Baia Mare area.

| Number | Weight % | | | | | | | | | |
|---|---|---|---|---|---|---|---|---|---|---|
| | **Bi** | **Pb** | **Te** | **Sb** | **Ag** | **Cu** | **Fe** | **Se** | **S** | **Total** |
| 1P Bi-1 | 45.64 | 29.46 | 0.17 | 0.01 | 5.49 | 1.03 | 0.55 | 0.15 | 16.61 | 99.11 |
| 1P Bi-2 | 46.79 | 30.70 | 0.11 | 0.04 | 5.25 | 0.99 | 0.42 | 0.11 | 16.45 | 100.86 |
| 1P Bi-3 | 45.34 | 30.46 | 0.24 | 0.11 | 5.43 | 0.64 | 0.26 | 0.13 | 16.40 | 99.01 |
| 196 Bi-1 | 50.89 | 22.17 | 0.19 | 0.12 | 7.59 | 1.69 | 0.68 | 0.23 | 17.09 | 100.65 |
| 196 Bi-2 | 51.26 | 22.70 | 0.21 | 0.10 | 7.52 | 0.63 | 0.15 | 0.28 | 16.87 | 99.72 |
| 196 Bi-3 | 51.64 | 19.16 | 0.15 | 0.18 | 9.07 | 0.59 | 0.05 | 0.30 | 16.90 | 98.04 |
| NV8 Bi-3 | 54.01 | 20.54 | 0.00 | 0.04 | 7.62 | 0.92 | 0.18 | 0.06 | 17.20 | 100.57 |
| NV9 Bi-1 | 47.78 | 27.20 | 0.11 | 0.07 | 5.77 | 0.88 | 0.25 | 0.21 | 16.59 | 98.86 |
| NV9 Bi-2 | 48.15 | 26.59 | 0.10 | 0.10 | 5.98 | 0.80 | 0.25 | 0.16 | 16.63 | 98.76 |
| 1P Bi-4 | 45.13 | 29.01 | 0.09 | 0.16 | 5.45 | 0.38 | 0.39 | 0.18 | 16.71 | 97.50 |
| 1P Bi-5 | 47.67 | 26.83 | 0.13 | 0.28 | 6.49 | 1.16 | 0.22 | 0.17 | 16.57 | 99.52 |
| 10D | 42.95 | 34.24 | 0.00 | 0.00 | 4.24 | 0.40 | 0.14 | 0.24 | 16.26 | 98.47 |
| 11D | 46.52 | 28.54 | 0.15 | 0.14 | 5.82 | 1.89 | 0.98 | 0.15 | 16.66 | 100.85 |
| 12D | 47.7 | 29.11 | 0.00 | 0.19 | 6.07 | 1.20 | 0.41 | 0.14 | 15.91 | 100.73 |
| 13D | 47.32 | 27.33 | 0.00 | 0.06 | 5.86 | 1.51 | 0.56 | 0.20 | 16.42 | 99.26 |
| 14D | 46.60 | 30.70 | 0.10 | 0.13 | 5.66 | 1.23 | 0.42 | 0.00 | 16.78 | 101.62 |
| 15D | 46.06 | 31.58 | 0.13 | 0.31 | 5.11 | 1.53 | 0.70 | 0.15 | 16.36 | 101.93 |
| 16D | 45.4 | 30.74 | 0.00 | 0.00 | 4.97 | 1.44 | 0.99 | 0.00 | 16.53 | 100.07 |
| 18D | 45.61 | 31.45 | 0.10 | 0.05 | 4.87 | 1.08 | 0.78 | 0.15 | 16.52 | 100.61 |
| 19D | 46.21 | 30.15 | 0.10 | 0.01 | 6.15 | 0.20 | 0.10 | 0.00 | 16.43 | 99.35 |
| 20D | 46.71 | 30.94 | 0.00 | 0.05 | 5.72 | 0.32 | 0.00 | 0.00 | 16.56 | 100.30 |
| 1P/1 | 46.48 | 29.81 | 0.14 | 0.11 | 5.54 | 1.17 | 0.67 | 0.05 | 16.50 | 100.47 |
| 1P/2 | 46.86 | 30.06 | 0.12 | 0.12 | 5.70 | 0.29 | 0.33 | 0.07 | 16.49 | 100.04 |
| 196/1 | 50.82 | 21.62 | 0.19 | 0.21 | 8.46 | 1.26 | 0.33 | 0.22 | 16.48 | 99.59 |
| N1/2 | 51.39 | 22.23 | 0.22 | 0.15 | 8.71 | 0.93 | 0.18 | 0.17 | 16.96 | 100.94 |
| N1/4 | 52.30 | 17.61 | 0.00 | 0.13 | 9.90 | 1.51 | 0.06 | 0.22 | 17.25 | 98.98 |
| N1/5 | 52.53 | 20.8 | 0.27 | 0.23 | 8.75 | 0.68 | 0.07 | 0.2 | 16.85 | 100.38 |
| N1/7 | 50.01 | 22.79 | 0.19 | 0.21 | 7.32 | 1.03 | 0.28 | 0.13 | 16.61 | 98.57 |

**Table 2.** *Cont.*

| Number | Weight % | | | | | | | | | | | |
|---|---|---|---|---|---|---|---|---|---|---|---|---|
| | **Bi** | **Pb** | **Te** | **Sb** | **Ag** | **Cu** | **Fe** | **Se** | **S** | | **Total** | |
| NV9/1 | 48.45 | 24.23 | 0.08 | 0.07 | 6.71 | 0.84 | 0.39 | 0.05 | 16.89 | | 97.71 | |
| **Chemical Formula on the Basis of 11 Atoms** | | | | | | | | | | | | |
| **Number** | **Bi** | **Pb** | **Te** | **Sb** | **Ag** | **Cu** | **Fe** | **Se** | **S** | **N** | **L** | **x** |
| 1P Bi-1 | 2.51 | 1.63 | 0.02 | 0.00 | 0.58 | 0.19 | 0.11 | 0.02 | 5.94 | 3.91 | 63.52 | 0.61 |
| 1P Bi-2 | 2.57 | 1.70 | 0.01 | 0.00 | 0.56 | 0.18 | 0.09 | 0.02 | 5.88 | 3.80 | 61.64 | 0.56 |
| 1P Bi-3 | 2.53 | 1.71 | 0.02 | 0.01 | 0.59 | 0.12 | 0.05 | 0.02 | 5.95 | 3.97 | 61.27 | 0.60 |
| 196 Bi-1 | 2.68 | 1.18 | 0.02 | 0.01 | 0.78 | 0.29 | 0.13 | 0.03 | 5.88 | 3.86 | 87.34 | 0.81 |
| 196 Bi-2 | 2.78 | 1.24 | 0.02 | 0.01 | 0.79 | 0.11 | 0.03 | 0.04 | 5.97 | 3.84 | 86.50 | 0.79 |
| 196 Bi-3 | 2.81 | 1.05 | 0.01 | 0.02 | 0.96 | 0.11 | 0.01 | 0.04 | 5.99 | 4.20 | 93.88 | 1.03 |
| NV8 Bi-3 | 2.89 | 1.11 | 0.00 | 0.00 | 0.79 | 0.16 | 0.04 | 0.01 | 6.00 | 3.56 | 96.42 | 0.75 |
| NV9 Bi-1 | 2.64 | 1.52 | 0.01 | 0.01 | 0.62 | 0.16 | 0.05 | 0.03 | 5.97 | 3.72 | 70.99 | 0.61 |
| NV9 Bi-2 | 2.66 | 1.48 | 0.01 | 0.01 | 0.64 | 0.15 | 0.05 | 0.02 | 5.98 | 3.73 | 73.09 | 0.63 |
| 1P Bi-4 | 2.51 | 1.63 | 0.01 | 0.02 | 0.59 | 0.07 | 0.08 | 0.03 | 6.07 | 3.91 | 63.82 | 0.61 |
| 1P Bi-5 | 2.61 | 1.48 | 0.01 | 0.03 | 0.69 | 0.21 | 0.04 | 0.02 | 5.91 | 3.97 | 72.56 | 0.72 |
| 10D | 2.43 | 1.96 | 0.00 | 0.00 | 0.47 | 0.07 | 0.03 | 0.04 | 6.00 | 3.93 | 48.90 | 0.47 |
| 11D | 2.48 | 1.54 | 0.01 | 0.01 | 0.60 | 0.33 | 0.20 | 0.02 | 5.80 | 3.91 | 66.89 | 0.64 |
| 12D | 2.64 | 1.63 | 0.00 | 0.02 | 0.65 | 0.22 | 0.08 | 0.02 | 5.74 | 3.94 | 67.37 | 0.65 |
| 13D | 2.59 | 1.51 | 0.00 | 0.01 | 0.62 | 0.27 | 0.11 | 0.03 | 5.86 | 3.80 | 70.32 | 0.63 |
| 14D | 2.51 | 1.67 | 0.01 | 0.01 | 0.59 | 0.22 | 0.08 | 0.00 | 5.90 | 3.97 | 62.52 | 0.62 |
| 15D | 2.49 | 1.72 | 0.01 | 0.03 | 0.54 | 0.27 | 0.14 | 0.02 | 5.77 | 3.86 | 58.98 | 0.55 |
| 16D | 2.47 | 1.69 | 0.00 | 0.00 | 0.52 | 0.26 | 0.20 | 0.00 | 5.86 | 3.81 | 59.48 | 0.54 |
| 18D | 2.49 | 1.73 | 0.01 | 0.00 | 0.51 | 0.19 | 0.16 | 0.02 | 5.88 | 3.80 | 58.06 | 0.52 |
| 19D | 2.58 | 1.70 | 0.01 | 0.00 | 0.67 | 0.04 | 0.02 | 0 | 5.98 | 4.16 | 64.25 | 0.69 |
| 20D | 2.59 | 1.73 | 0.00 | 0.00 | 0.62 | 0.06 | 0.00 | 0.00 | 5.99 | 4.00 | 62.34 | 0.62 |
| 1P/1 | 2.53 | 1.64 | 0.01 | 0.01 | 0.59 | 0.21 | 0.14 | 0.01 | 5.86 | 3.88 | 63.79 | 0.60 |
| 1P/2 | 2.60 | 1.68 | 0.01 | 0.01 | 0.61 | 0.05 | 0.07 | 0.01 | 5.96 | 3.93 | 64.04 | 0.62 |
| 196/1 | 2.75 | 1.18 | 0.02 | 0.02 | 0.89 | 0.22 | 0.07 | 0.03 | 5.82 | 4.17 | 87.72 | 0.95 |
| N1/2 | 2.74 | 1.20 | 0.02 | 0.01 | 0.90 | 0.16 | 0.04 | 0.02 | 5.90 | 4.26 | 86.73 | 0.98 |
| N1/4 | 2.77 | 0.94 | 0.00 | 0.01 | 1.02 | 0.26 | 0.01 | 0.03 | 5.95 | 4.39 | 96.97 | 1.16 |
| N1/5 | 2.83 | 1.13 | 0.02 | 0.02 | 0.91 | 0.12 | 0.01 | 0.03 | 5.92 | 4.09 | 91.39 | 0.95 |
| N1/7 | 2.74 | 1.26 | 0.02 | 0.02 | 0.78 | 0.19 | 0.06 | 0.02 | 5.93 | 3.87 | 84.83 | 0.79 |
| NV9/1 | 2.66 | 1.34 | 0.01 | 0.01 | 0.71 | 0.15 | 0.08 | 0.01 | 6.04 | 3.84 | 79.49 | 0.73 |

Lillianite-gustavite appears as submicroscopic grains included in chalcopyrite and quartz and rarely in pyrite. Most of the lillianite-gustavite crystals are frequently associated with native gold of high fineness. Microscopic lillianite-gustavite lamellae frequently appear in the form of granular intergrowths with members of the bismuthinite-aikinite series (pekoite and krupkaite) (Figure 4a) and subordinately with areas whose composition most closely resembles bismuthinite (Figure 4b). There are also lillianite-gustavite crystal inclusions in chalcopyrite that contain heterogeneous lath-like domains with a composition characteristic of matildite and bismuthinite (Figure 4c) (Sample 8NV/1 in Table 1). These observations explain the compositional variation during growth, accepted by the structure

of these minerals series [15]. The appearance of the intergrowths between the minerals from the two mineral series indicates that these minerals were deposited towards the final stages of paragenetic mineralization and are not the result of exsolutions. Most of the lillianite-gustavite crystals situated at the border between chalcopyrite and quartz (Figure 4d–f) are compositionally homogenous and belong to the $Gus_{73.08–59.48}$ miscible area (Table 2). Such homogenous compositions could be the result of fast cooling [60]. Fine layers of wittichenite are found around some lillianite-gustavite crystals associated with gold included in chalcopyrite (Figure 6c) or in quartz (Figure 6a).

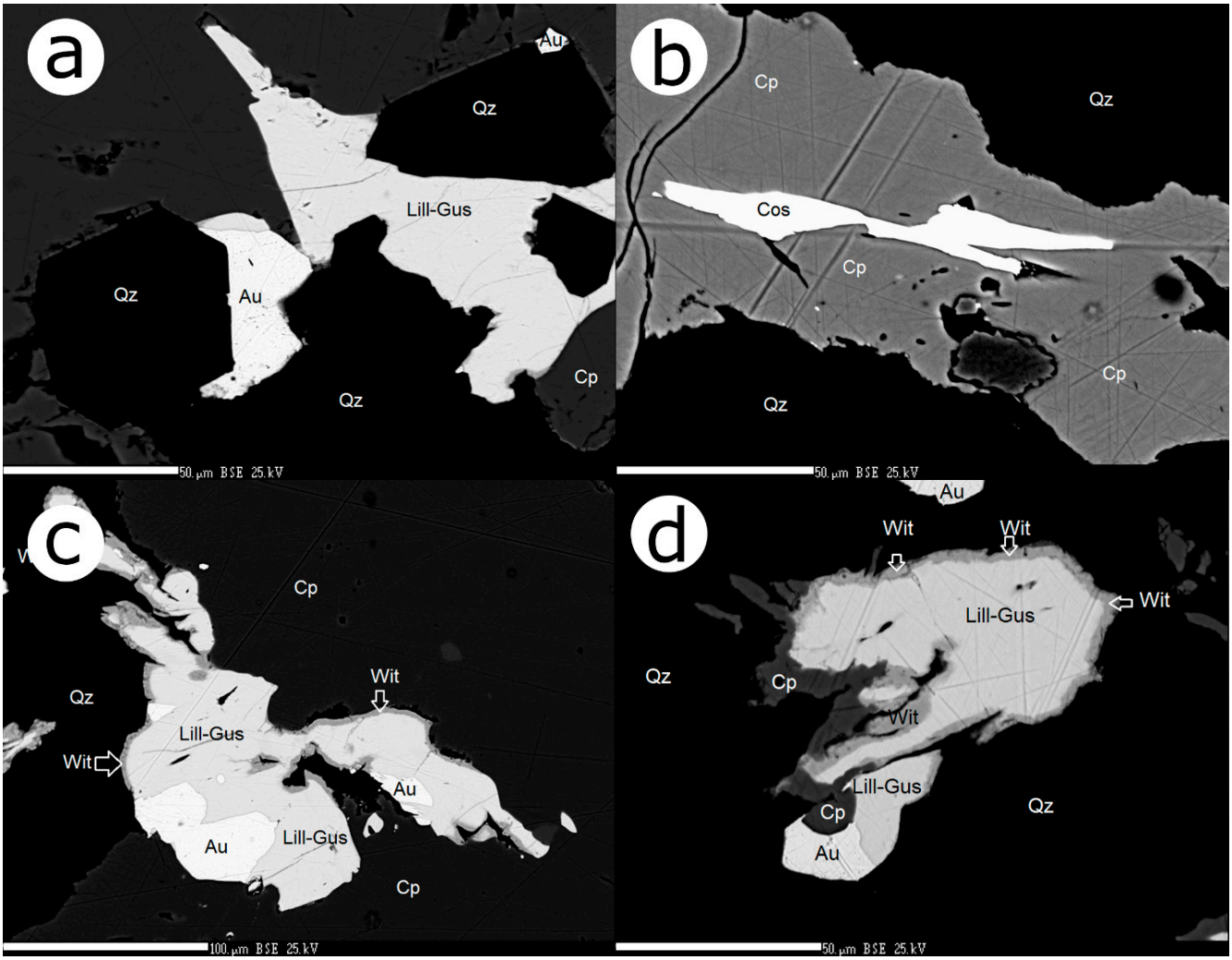


**Figure 6.** (**a**) Lillianite-Gustavite and native gold as inclusions on the boundaries between chalcopyrite and idiomorphic quartz. (**b**) Lamellar cosalite within chalcopyrite in a matrix of quartz. (**c**) Lillianite-gustavite–native gold assemblage bordered by wittichenite located at boundaries between quartz and chalcopyrite. (**d**). Wittichenite as rims around lillianite-gustavite crystals and between relict crystals of chalcopyrite included in quartz; Abbreviations: Au—native gold, Cos—cosalite, Cp—chalcopyrite, Lill-Gus—lillianite-gustavite, Qz—quartz, Wit—wittichenite.

The chemical composition of the majority of the samples from the Nistru deposit (Table 2) confirmed the presence of Bi-Ag-rich members of the lillianite-gustavite series (Figure 3). We note that compositions close to gustavite ($Gus_{96.96}$-$Gus_{79.48}$) are dominant (Figure 7), while those positioned mid-way along the series ($Gus_{48.90}$) are subordinate (Table 2). In the majority of analyses, Cu contents are below 1.89 wt.%. Such levels of Cu can be incorporated into the lillianite-gustavite structure via different substitution mechanisms [28]. Concentrations of Sb (as low as 0.31 wt.%) substituting for Bi and Fe

(never exceeding 0.99 wt.%) were probably in the Pb site. The contents of Se and Te as substitutes for S have maximum concentrations of 0.30 and 0.23 wt.%, respectively. Similar compositions were observed by Cook [12] at Baia Borsa, Voudouris et al. [25] in the Stanos deposit, Greece and by Bristol et al. [23] at Chalkidiki, northern Greece. The general crystallochemical formula is:

$$Pb_{0.94–1.96}Bi_{2.43–2.89}Ag_{0.47–1.02}Cu_{0–0.29}Fe_{0.0–0.20}Sb_{0–0.3}Te_{0.0–0.03}Se_{0.0–0.04}S_{5.77–6.07}$$

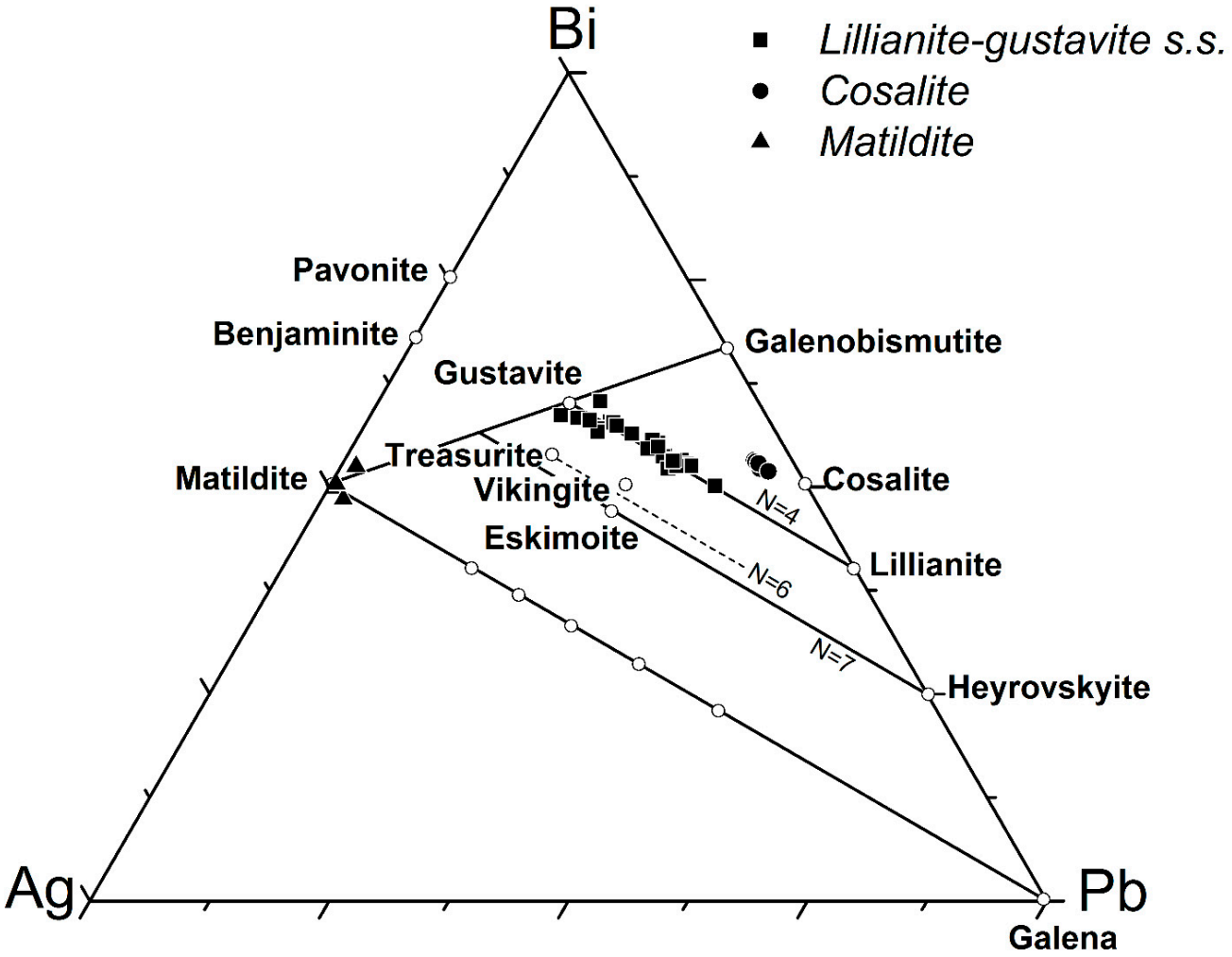


**Figure 7.** Compositional data for lillianite homologs plotted on a Pb-Bi-Ag ternary diagram (atom.%).

5.2.3. Matildite

Compositional data and empirical formulae are given in Table 3. In the ternary Bi-Ag-Pb diagram (Figure 7), matildite occurrence is a result of the calculated composition rich in Ag and Bi. The chemical composition of matildite is slightly different from the ideal one according to Harris and Thorpe (1969) and Voudouris et al. [25,61] because of the Cu and Pb content. In a sample from the same paragenetic sequence, Plotinskaya et al. [38] described an association of matildite with tetradymite and native gold. Matildite is also present as laths enclosed in the gustavite matrix (Figure 4c). The occurrence of matildite from Nistru is completely different from the Suior Baia Mare area [36] and from the Bieber vein, Banská Štiavnica deposit, Slovakia [11], where it characteristically occurs as myrmekitic intergrowth with galena.

**Table 3.** EPMA data for matildite, cosalite and wittichenite.

| Number | Weight % | | | | | | | | | |
|---|---|---|---|---|---|---|---|---|---|---|
| | **Bi** | **Pb** | **Te** | **Sb** | **Ag** | **Cu** | **Fe** | **Se** | **S** | **Total** |
| *Matildite* | | | | | | | | | | |
| 21D | 53.44 | 1.60 | 0.00 | 0.10 | 24.13 | 1.43 | 0.15 | 0.12 | 15.43 | 96.40 |
| 22D | 51.71 | 0.20 | 0.00 | 0.56 | 26.74 | 1.44 | 0.12 | 0.10 | 15.82 | 96.69 |
| N1/10 | 52.43 | 2.39 | 0.04 | 0.11 | 27.46 | 0.55 | 0.03 | 0.04 | 17.42 | 100.47 |
| N1/11 | 53.12 | 0.64 | 0.07 | 0.05 | 26.76 | 0.24 | 0.02 | 0.07 | 17.11 | 98.08 |
| *Cosalite* | | | | | | | | | | |
| 23D | 43.82 | 36.54 | 0.44 | 0.10 | 1.68 | 2.37 | 0.67 | 0.00 | 16.60 | 102.22 |
| 24D | 42.65 | 34.06 | 0.12 | 0.16 | 1.64 | 2.11 | 0.54 | 0.22 | 16.35 | 97.85 |
| 25D | 43.98 | 35.42 | 0.00 | 0.24 | 1.66 | 1.83 | 0.44 | 0.15 | 16.33 | 100.05 |
| 26D | 43.26 | 35.32 | 0.09 | 0.18 | 1.56 | 1.88 | 0.56 | 0.20 | 16.36 | 99.41 |
| NV8 Bi-4 | 42.18 | 36.27 | 0.02 | 0.15 | 1.32 | 2.36 | 0.81 | 0.06 | 16.69 | 99.86 |
| *Wittichenite* | | | | | | | | | | |
| 1P Bi-6 | 40.32 | 0.89 | 0.08 | 0.22 | 3.18 | 32.66 | 1.66 | 0.31 | 19.80 | 99.12 |
| 1P/3 | 41.28 | 1.02 | 0.20 | 0.29 | 2.94 | 32.44 | 0.29 | 0.21 | 19.42 | 98.09 |
| NV6/1 | 39.71 | 0.24 | 0.00 | 0.09 | 3.67 | 34.29 | 0.37 | 0.01 | 20.00 | 98.38 |
| **Empirical Chemical Formula** | | | | | | | | | | |
| **(The formulae were calculated based on: 4 atoms (matildite), 36 atoms (cosalite), and 7 atoms (wittichenite)** | | | | | | | | | | |
| **Number** | **Bi** | **Pb** | **Te** | **Sb** | **Ag** | **Cu** | **Fe** | **Se** | **S** | |
| *Matildite* | | | | | | | | | | |
| 21D | 1.03 | 0.031 | 0.000 | 0.003 | 0.898 | 0.090 | 0.011 | 0.006 | 1.933 | |
| e22D | 0.970 | 0.004 | 0.000 | 0.018 | 0.972 | 0.089 | 0.008 | 0.005 | 1.934 | |
| N1/10 | 0.937 | 0.043 | 0.001 | 0.003 | 0.951 | 0.032 | 0.002 | 0.002 | 2.029 | |
| N1/11 | 0.973 | 0.012 | 0.002 | 0.002 | 0.949 | 0.015 | 0.002 | 0.004 | 2.042 | |
| *Cosalite* | | | | | | | | | | |
| 23D | 7.759 | 6.526 | 0.128 | 0.030 | 0.576 | 1.380 | 0.444 | 0.000 | 19.157 | |
| 24D | 7.804 | 6.285 | 0.036 | 0.050 | 0.581 | 1.270 | 0.370 | 0.107 | 19.498 | |
| 25D | 8.003 | 6.501 | 0.000 | 0.075 | 0.585 | 1.095 | 0.300 | 0.072 | 19.368 | |
| 26D | 7.874 | 6.484 | 0.027 | 0.056 | 0.550 | 1.125 | 0.381 | 0.096 | 19.407 | |
| NV8 Bi-4 | 7.544 | 6.543 | 0.006 | 0.045 | 0.456 | 1.386 | 0.539 | 0.029 | 19.452 | |
| *Wittichenite* | | | | | | | | | | |
| 1P Bi-6 | 0.969 | 0.021 | 0.003 | 0.009 | 0.148 | 2.580 | 0.149 | 0.019 | 3.101 | |
| 1P/3 | 1.019 | 0.025 | 0.008 | 0.012 | 0.141 | 2.632 | 0.027 | 0.013 | 3.122 | |
| NV6/1 | 0.953 | 0.006 | 0.000 | 0.004 | 0.170 | 2.705 | 0.034 | 0.001 | 3.127 | |

#### 5.2.4. Cosalite

Cosalite was optically identified as lamellar crystals included in chalcopyrite (Figure 6b; Sample NV-8). Compositionally, the phase is reasonably close to ideal stoichiometry (Table 3, Figure 7) albeit with 1.31 to 1.68 wt.% Ag and 1.83 to 2.37 wt.% Cu). Comparable Ag and Cu contents are reported by Voudouris et al. [25], Pazout et al. [4] and Mederski et al. [20]. The formation of cosalite together with lillianite homologs may be due to the Cu content, which is less readily incorporated into the lillianite structure [62].

The presence of Cu in solution can cause the destabilization of gustavite and the formation of cosalite [63]. A substitution mechanism for Cu in cosalite was described by Topa and Makovicky [64].

#### 5.2.5. Wittichenite

Wittichenite is a minor phase and appears as fine rims around lillianite-gustavite grains (Figure 6c,d) (Sample 1P-6). From a compositional point of view, due to the silver content (3.67 wt.%) (Table 3), it should belong to a silver-rich stage according to Xiang-Ping et al. [22]. In the paragenesis described by Jeleň et al. [13], wittichenite with an even higher amount of silver up to 6.3 wt.% is presented as a secondary phase replacing aikinite. Alteration rims of wittichenite with 1.6 wt.% Ag surrounding matildite were described by Cook [34] from Bi-sulfosalts in the Văratec mineralization at Băiuț.

### *5.3. Fluid Inclusion Data*

The formation temperature for the Cu+Bi+Au vein was estimated from a fluid inclusions study. The examination of a great number of double-polished plates allowed us to find primary fluid inclusions greater than 15 μm in size in quartz, which were suitable for the investigation. Primary, pseudo-secondary and secondary inclusions were recognized according to criteria given by Roedder [65]. The primary fluid inclusions are regularly distributed in host quartz or occur along growth zones, while secondary inclusions heal fractures, cutting the host mineral. The pseudo-secondary fluid inclusions heal the fractures within crystals, but these fractures do not reach the crystal surface; at the same time, the phase composition of these inclusions is similar to that of primary inclusions.

Only two-phase gaseous-liquid inclusions were found during the visual examination of fluid inclusions in quartz hosting Bi-sulfosalts from the Nistru deposit (Figure 8). The coexistence of liquid and gaseous inclusions suggests an effervescence phenomenon [66]. For thermo- and cryometric investigations, we chose fluid inclusions that were uniformly distributed over the quartz volume and could therefore be confidently classified as primary inclusions.

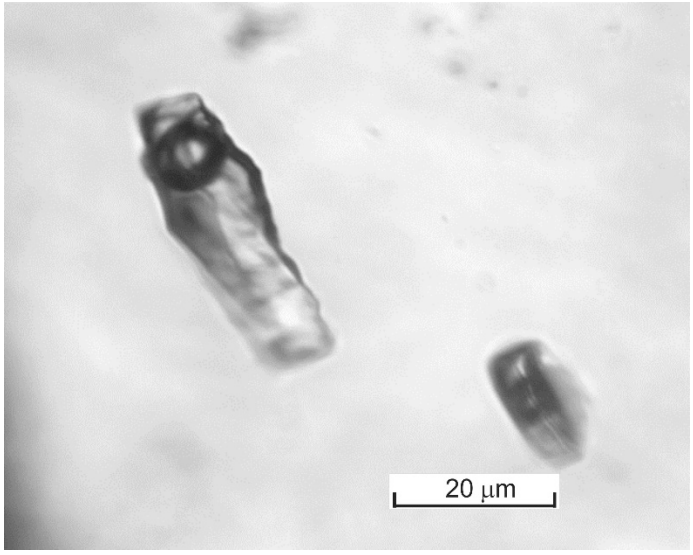


**Figure 8.** Two-phase fluid inclusions within mineralized quartz vein containing Bi-minerals.

The results of thermo- and cryometric investigations of (n = 36) individual fluid inclusions in quartz of the studied vein (Table 4, Figure 9) indicated the dominance of NaCl, KCl and MgCl among the two-phase fluid solutions of admixtures. This is evidenced by chloride eutectics of the admixture solutions in the temperature interval from −21 to −35 °C (Table 4). Complete homogenization of the fluid admixtures takes place

in a narrow temperature interval (from 205 to 247 °C). Salinities vary between 0.4 and 2.6 wt.% NaCl equivalent. The density of the fluid changes from 0.8 to 0.87 g/cm$^3$. A slight increase in salinity as temperature decreases is noted (Table 4), with higher temperatures corresponding to lower salinity. The very low salinity would suggest that mixing between hydrothermal solutions and meteoric water was an important mechanism for the successive deposition of the mineral components.

**Table 4.** Microthermometric data for fluid inclusions in quartz (sample N1, Nistru deposit).

| Index № | n | $T_{hom}$, °C | $T_{eut}$, °C | $T_{ice\ melt}$, °C | wt. % eq. NaCl | d, g/sm$^3$ |
|---|---|---|---|---|---|---|
| 1 | 3 | 225 | −27 | −1.5 | 2.6 | 0.86 |
| 2 | 7 | 222 | −35 | −1.4 | 2.4 | 0.86 |
| 3 | 3 | 227 | −26 | −0.5 | 0.9 | 0.84 |
| 4 | 3 | 239 | −22 | −0.8 | 1.4 | 0.82 |
| 5 | 2 | 247 | −28 | −0.5 | 0.9 | 0.80 |
| 6 | 3 | 224 | −22 | −1.1 | 1.9 | 0.85 |
| 7 | 2 | 241 | −23 | −0.6 | 1.1 | 0.82 |
| 8 | 2 | 219 | −21 | −0.6 | 1.1 | 0.85 |
| 9 | 3 | 210 | −22 | −0.8 | 1.4 | 0.87 |
| 10 | 3 | 207 | −23 | −0.7 | 1.2 | 0.87 |
| 11 | 2 | 205 | −21 | −0.3 | 0.5 | 0.86 |
| 12 | 3 | 207 | −22 | −0.2 | 0.4 | 0.86 |

Total number of studied inclusions = 36; d—fluid density.

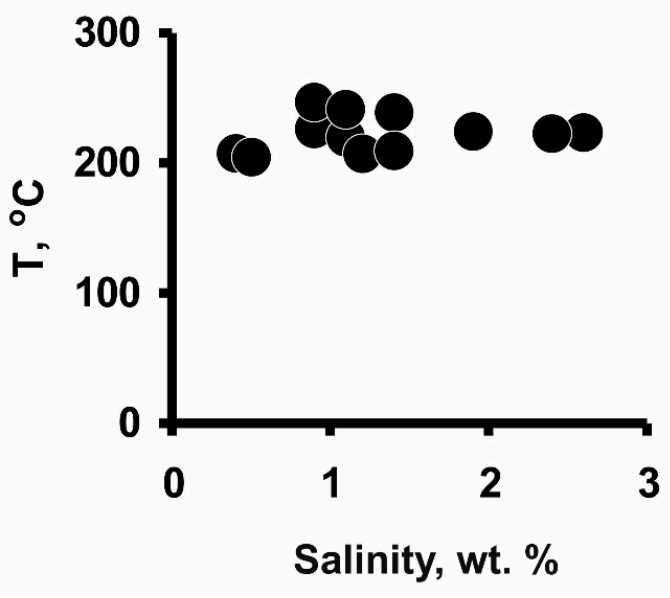


**Figure 9.** Temperature versus salinity diagram for ore-forming fluids (sample N1).

## 6. Discussion and Conclusions

Although preliminary data for Bi-minerals from Cu ores rich in native gold from the Nistru deposit have been reported previously [37,67], the interpretations presented here are based on a larger, more representative EPMA dataset. Observations and analytical results contribute to understanding the important relationship between native gold, Bi-sulfosalts and the main sulfides, and also highlight the widespread intergrowths and compositional

variations present within individual Bi-sulfosalt series. Fluid inclusion geothermometry allows constraints to be placed on the conditions of ore formation.

The occurrence of Bi-sulfosalts and native gold within a copper vein from the SE area emphasizes the marked gold enrichment in hydrothermal mineralization from the western part of the Baia Mare metallogenetic district.

Bismuth sulfosalts are represented by bismuthinite derivatives and members of the lillianite homologous series. Compositions of the latter extend over lillianite and gustavite ($^4$N species). Cosalite is also present as are subordinate amounts of matildite and wittichenite.

The Bi-sulfosalts occur within a quartz-pyrite-chalcopyrite vein rich in native gold. Sphalerite and subordinate pyrrhotite and arsenopyrite are also present. The Cu+Bi+Au vein is hosted in the apophysis of a shallow subvolcanic stock comprising porphyry quartz-micromonzodiorite, from the SE part of the Nistru deposit. The copper vein is part of a zonation of the Nistru deposit, whereby deeper levels are associated with a possible "porphyry copper" system. This hypothesis is emphasized by the presence of a pervasive potassic alteration in the subvolcanic body (potassic feldspar, biotite, sericite) together with chalcopyrite. These preliminary observations have been sustained by Baksheev et al. [68]. The chemical composition of phlogopite, tourmaline and illite from altered rocks of the Nistru Cu-Au-Bi deposit suggests that the Nistru deposit is of porphyry type with epithermal-style mineralization at upper levels. Compared to data presented by Xu et al. [69] the association of the potassic metasomatism with chalcopyrite and magnetite could be evidence for a hypogene porphyry copper genetic model.

Data regarding formation temperatures for the quartz vein hosting Bi-sulfosalts were given by Damian [37], who obtained homogenization temperatures of fluid inclusions in quartz between 230 and 240 °C. Damian [44] also detected the presence of invisible gold within nine grains of pyrite by secondary ion mass spectrometry. Measured concentrations ranged from 0.16 to 64 ppm Au, with an average of 33.4 ppm Au. The average As content was 1.1%. After Arehart et al. [70], gold was deposited in pyrite as a solid solution coupled with As. The upper solubility limit for a solid solution of Au and As in arsenian pyrite ranges between 150 and 250 °C [71]. Plotinskaya et al., [38], estimatesd a very small stability field for 300 °C and a larger field for 200 °C for the presence of tetradymite (intergrown with native gold and matildite) in the Cu-Bi-Au (Nistru) mineralization, in diagram $fS_2$-$fTe_2$ for galena and bismuth minerals. Based on the FeS content of sphalerite associated with pyrrhotite, chalcopyrite and pyrite in Cu-Bi-Au (Nistru) mineralization, Plotinskaya et al. [54] proposes a temperature decrease from >300° to 200 °C, specific for the Py-Po buffer on a $fS_2$-T diagram. The presence of pyrrhotite within the mineral assemblage indicates Py-Po equilibrium at hydrothermal conditions between 200 and 400 °C following Marcoux et al. [72].

The low salinity of fluid and the temperatures below 300 °C suggest an epithermal system [66,73]. Temperature values and low salinities are comparable to those obtained by Prokofiev et al. [74] and Kovalenker et al. [75] for epithermal mineralization in Banska Štiavnica, Central Slovakia. Cook [12] estimates temperatures of over 350 °C, even up to 450 °C for the Toroiaga (Baia Borșa) vein system, in the case of the formation of the homologs series of lillianite. Therefore, comparing it with the maximum temperature (247 °C) obtained through fluid inclusion, it could be appreciated that the Bi-sulfosalts in Nistru area may have formed at a lower temperature than those in Toroiaga, probably also due to the relatively shallow position of the subvolcanic bodies in the Nistru zone. We appreciate that the upper-temperature limit of Bi-sulfosalt formation may exceed 300 °C, based on [54], and up to 247 °C, according to data obtained in this study [37,67]. These temperatures are similar to those obtained by Voudouris et al. from the Perama Hill high-sulfidation epithermal system (221–331 °C and low salinity up to 4.9 wt.% NaCl equivalent) [9]. Bristol et al. [23] obtained a temperature range between 170 and 350 °C within a shear zone type mineralization, and Yue et al. [76] obtained temperatures

of 210–290 °C in a a hydrothermal deposit containing bismuth mineral assemblages similar to those in Nistru.

Native gold associated with Bi-sulfosalts has a relatively low Ag content [37,38]. The sporadic presence of tetradymite has also been emphasized in this mineralogical assemblage [38]. The formation of Bi-sulfosalts is favored by a progressive decrease in the sulfur fugacity [38,77].

The presence of bismuth minerals in association with native gold and sulfides is significant for the role of subvolcanic intrusions in the metallogenetic processes [78], and it places the rich in gold cupriferous sequence with Bi-sulfosalts in the Nistru zone, Baia Mare to the intermediate sulfidation type. The Bi-minerals vein in the Nistru zone represents an example of a low-salinity copper-gold deposit associated with a subvolcanic intrusion in an area of subduction [45]. Cioflica et al. [79] include the Neogene gold mineralization from Romania as a gold-bearing base metal sulfides deposit related to the meso-epithermal stage. The presence of an assemblage rich in Bi- and Ag-sulfosalts reflects the role of a nearby magmatic source [8], which in Nistru is very obvious. Kołodziejczyk et al. [18] obtained temperatures from 250 to 350 °C for bismuth mineral phases in the Stan Terg deposit (Trepça, Kosovo), corresponding to a hydrothermal system of low-sulfidation type.

The gold-bismuth sulfosalt occurrence from Nistru in the western part of Baia Mare metalogenetic district could add significantly to the understanding of hydrothermal processes associated with Neogene magmatism, in comparison with other occurrences of Bi-sulfosalts without gold, as in Suior [36] and Baia Sprie [10].

**Author Contributions:** Conceptualization, G.D., N.J.C. and F.D.; methodology, F.D., N.J.C., V.Y.P. and P.A.; validation, F.D., N.J.C. and G.D.; formal analysis, G.D., P.A. and V.Y.P.; investigation, N.J.C. and G.D.; resources, G.D.; data curation, F.D.; draft preparation, F.D.; writing—review and editing, N.J.C.; visualization, F.D.; project administration, G.D.; funding acquisition, G.D. and P.A. All authors have read and agreed to the published version of the manuscript.

**Funding:** This work was supported by the Carpathian Association of Environment and Earth Sciences, Baia Mare Romania.

**Data Availability Statement:** Data are contained within the article.

**Acknowledgments:** Thanks are also extended to the electron microanalysis staff at IGEM-RAS (Moscow) and the State Geological Institute of Dionyz Stur (Bratislava, Slovakia) for their analytical support.

**Conflicts of Interest:** The authors declare no conflicts of interest.

## References

1. Borodaev, Y.S.; Garavelli, A.; Garbarino, C.; Grillo, S.M.; Mozgova, N.N.; Paar, W.H.; Topa, D.; Vurro, F. Rare Sulfosalts from Vulcano, Aeolian Islands, Italy. V. Selenian Heyrovskyite. *Can. Mineral.* **2003**, *41*, 429–440. [CrossRef]
2. Marquez-Zavalia, M.F.; Galliski, M.A.; Cerny, P.; Chapman, R. An Assemblage of Bismuth-Rich, Tellurium-Bearing Minerals in the El Quemado Granitic Pegmatite, Nevados De Palermo, Salta, Argentina. *Can. Mineral.* **2013**, *50*, 1489–1498. [CrossRef]
3. Meng, L.; Huang, F.; Gao, W.; Gao, R.; Zhao, F.; Zhou, Y.; Li, Y. Multi-Step Gold Refinement and Collection Using Bi-Minerals in the Laozuoshan Gold Deposit, NE China. *Minerals* **2022**, *12*, 1137. [CrossRef]
4. Pažout, R. Lillianite homologues from Kutná Hora ore district, Czech Republic: A case of large-scale Sb for Bi substitution. *J. Geosci.* **2017**, *62*, 37–57. [CrossRef]
5. Pažout, R.; Sejkora, J.; Šrein, V. Bismuth and bismuth-antimony sulphosalts from Kutná Hora vein Ag-Pb-Zn ore district, Czech Republic. *J. Geosci.* **2017**, *62*, 59–76. [CrossRef]
6. Števko, M.; Sejkora, J. Bismuth, lead-bismuth and lead-antimony sulfosalts from the granite-hosted hydrothermal quartz veins at the Elisabeth mine, Gemerská Poloma, Spišsko-gemerské rudohorie Mts., Slovakia. *J. Geosci.* **2021**, *66*, 157–173. [CrossRef]
7. Zhou, H.; Sun, X.; Wu, Z.; Yang, T.; Li, D.; Ren, Y.; Liu, Q.; Zhu, K.; Yu, H. Mineralogy of Bi-sulfosalts and tellurides from the Yaoan gold deposit, southwest China: Metallogenic implications. *Ore. Geol. Rev.* **2018**, *98*, 126–140. [CrossRef]
8. Marcoux, E.; Milesi, J.P.; Sohearto, S.; Rinawan, R. Noteworthy mineralogy of the Au-Ag-Sn-W(Bi) epithermal ore deposit of Cirotan, West Java, Indonesia. *Can. Mineral.* **1993**, *31*, 727–744.
9. Voudouris, P.C.; Melfos, V.; Spry, P.G.; Moritz, R.C.; Papavassiliou, C.; Falalakis, G. Mineralogy and geochemical environment of formation of the Perama Hill high-sulfidation epithermal Au-Ag-Te-Se deposit, Petrota Graben, NE Greece. *Min. Pet.* **2011**, *103*, 79–100. [CrossRef]

10. Buzatu, A.; Damian, G.; Dill, H.G.; Buzgar, N.; Apopei, A.I. Mineralogy and geochemistry of sulfosalts from Baia Sprie ore deposit (Romania)—New bismuth minerals occurrence. *Ore Geol. Rev.* **2015**, *65*, 132–147. [CrossRef]
11. Chovan, M.; Mikuš, T.; Prcúch, J.; Bača, B. Assemblage of Ag–Pb–Bi±Cu sulfosalts from the Bieber vein, Banská Štiavnica deposit, Slovakia. *Acta Geol. Slovaca* **2021**, *13*, 191–198.
12. Cook, N.J. Bismuth and bismuth-antimony sulphosalts from Neogene vein mineralization, Baia Borşa area, Maramureş, Romania. *Mineral. Mag.* **1997**, *61*, 387–409. [CrossRef]
13. Jelen, S.; Prsek, J.; Kovalenker, V.A.; Topa, D.; Sejkora, J.; Stevko, M.; Ozdin, D. Bismuth Sulfosalts of the Cuprobismutite, Pavonite and Aikinite Series from the Rozalia Mine, Hodrusa-Hamre, Slovakia. *Can. Mineral.* **2012**, *50*, 325–340. [CrossRef]
14. Kouzmanov, K.; Bogdanov, K.; Ramboz, C. Te- and Bi-bearing assemblages in the Elshitsa and Radka epithermal deposits, Central Srednogorie, Bulgaria: Mineralogy and genetical features. *Mineral. Petrol. Sofia* **2005**, *43*, 108–112.
15. Ciobanu, C.L.; Cook, N.J. Intergrowths of bismuth sulphosalts from the Ocna de Fier Fe-skarn deposit, Banat, Southwest Romania. *Eur. J. Mineral.* **2000**, *12*, 899–917. [CrossRef]
16. Cioflica, G.; Jude, R.; Lupulescu, M.; Simon, G.; Damian, G. New data on the Bi-minerals from the mineralizations related to Paleocene magmatites in Romania. *Rom. J. Mineral.* **1995**, *72*, 9–23.
17. Dana, C.D.P.; Agangi, A.; Idrus, A.; Lai, C.-K.; Simbolon, D.R. Bi-Ag-Sulfosalts and Sulfoarsenides in the Ruwai Zn-Pb-Ag Skarn Deposit, Central Borneo, Indonesia. *Minerals* **2022**, *12*, 1564. [CrossRef]
18. Kołodziejczyk, J.; Pršek, J.; Melfos, V.; Voudouris, P.C.; Maliqi, F.; Kozub-Budzyń, G. Bismuth minerals from the Stan Terg deposit (Trepça, Kosovo). *Neues Jahrb. Mineral. Abh.* **2015**, *192*, 317–333. [CrossRef]
19. Kołodziejczyk, J.; Pršek, J.; Voudouris, P.C.; Melfos, V. Bi-sulphotellurides associated with Pb-Bi-(Sb ± Ag, Cu, Fe) sulphosalts: An example from the Stan Terg deposit in Kosovo. *Geol. Carpathica* **2017**, *68*, 366–381. [CrossRef]
20. Mederski, S.; Pršek, J.; Dimitrova, D.; Hyseni, B. A Combined EPMA and LA-ICP-MS Investigation on Bi-Cu-Au Mineralization from the Kizhnica Ore Field (Vardar Zone, Kosovo). *Minerals* **2021**, *11*, 1223. [CrossRef]
21. Mederski, S.; Pršek, J.; Kołodziejczyk, J.; Kluza, K.; Melfos, V.; Adamek, K.; Dimitrova, D. Mineralogical and geochemical studies of Cu-Bi-Ag±W ores from Janjevo (Kosovo): Insights into the Bi sulfosalt mineralogy and the distribution of bismuth in base metal sulfides. *J. Geosci.* **2023**, *68*, 139–162. [CrossRef]
22. Xiang-Ping, G.; Watanabe, M.; Ohkawa, M.; Hoshino, K.; Shibata, Y.; Desong, C. Felbertalite and Related Bismuth Sulfosalts from the Funiushan Copper Skarn Deposit, Nanjing, China. *Can. Mineral.* **2001**, *39*, 1641–1652. [CrossRef]
23. Bristol, S.K.; Spry, P.G.; Voudouris, P.C.; Melfos, V.; Mathur, R.D.; Fornadel, A.P.; Sakellaris, G.A. Geochemical and geochronological constraints on the formation of shear-zone hosted Cu-Au-Bi-Te mineralization in the Stanos area, Chalkidiki, northern Greece. *Ore. Geol. Rev.* **2015**, *66*, 266–282. [CrossRef]
24. Ciobanu, C.L.; Cook, N.J.; Damian, F.; Damian, G. Gold scavenged by bismuth melts: An example from Alpine shear-remobilizates in the Highiş Massif, Romania. *Mineral. Petrol.* **2006**, *87*, 351–384. [CrossRef]
25. Voudouris, P.C.; Spry, P.G.; Mavrogonatos, C.; Sakellaris, G.A.; Bristol, S.K.; Melfos, V.; Fornadel, A.P. Bismuthinite derivatives, lillianite homologues, and bismuth sulfotellurides as indicators of gold mineralization in the Stanos shear-zone related deposit, Chalkidiki, northern Greece. *Can. Mineral.* **2013**, *51*, 119–142. [CrossRef]
26. Makovicky, E. Modular crystal chemistry of sulphosalts ans other complex sulphides. In *European Mineralogical Union, Notes in Modular Aspects of Minerals*; Merlino, S., Ed.; European Mineralogical Union: Dublin, Ireland, 1997; Volume 1, pp. 237–271. ISBN 9780903056472. [CrossRef]
27. Chen, T.T.; Kirchner, E.; Paar, W. Friedrichite Cu5Pb5Bi7S18 a new member of the aikinite-bismuthinite series. *Can. Mineral.* **1978**, *16*, 1127–1130.
28. Makovicky, E.; Karup-Møller, S. Chemistry and crystallography of the lillianite homologous series, Part I: General properties and definitions. *Neues Jahrb. Mineral. Abh.* **1977**, *130*, 264–287.
29. Makovicky, E.; Karup-Møller, S. Chemistry and crystallography of the lillianite homologous series, Part II: Definition of new minerals: Eskimoite, vikingite, ourayite and treasurite. Redefinition of schirmerite and new data on the lillianite-gustavite solid-solution series. *Neues Jahrb. Mineral. Abh.* **1977**, *131*, 56–82.
30. Moëlo, Y.; Makovicky, E.; Mozgova, N.N.; Jambor, J.L.; Cook, N.; Pring, A.; Paar, W.; Nickel, E.H.; Graeser, S.; Karup-Møller, S.; et al. Sulfosalt systematics: A review. Report of the sulfosalt sub-committee of the IMA Commission on Ore Mineralogy. *Eur. J. Mineral.* **2008**, *20*, 7–62. [CrossRef]
31. Zajzon, N.; Szentpéteri, K.; Fehér, B.; Szakáll, S.; Kristály, F. Krupkaite from Avram Iancu mine, Băiţa (Bihor) metallogenic district, Romania. In Proceedings of the Joint 5th Mineral Sciences in the Carpathians Conference and 3rd Central-European Mineralogical Conference, Miskolc, Hungary, 20–21 April 2012; University of Miskolc: Miskolc, Hungary, 2012.
32. Ilinca, G. Rare sulphosalt minerals in Romania. *Acta Mineral.-Petrogr* **2006**, *5*, 42–46.
33. Ciobanu, C.L.; Pring, A.; Cook, N.J. Micron-to nano-scale intergrowths among members of the cuprobismutite series and paděraite: HRTEM and microanalytical evidence. *Mineral. Mag.* **2004**, *68*, 279–300. [CrossRef]
34. Cook, N.J. Bismuth sulphosalts from hydrothermal vein deposits of Neogene Age, N.W. Romania. *Mitt. Osterr. Miner. Ges.* **1998**, *143*, 19–39.
35. Costin, D.; Vlad, S. Ore formation at Varatec-Baiut (Baia Mare region, East Carpathians Romania. *Geochem. Mineral. Petrol.* **2005**, *43*, 64–68.

36. Damian, G.; Ciobanu, C.L.; Cook, N.J.; Damian, F. Bismuth sulphosalts from the galena-matildite series in the Cremenea vein, Şuior, Baia Mare district, Romania. *Neues Jahrb. Mineral. Abh.* **2008**, *185*, 199–213. [CrossRef]
37. Damian, F. Bismuth minerals-native gold association in the copper mineralisation from Nistru-Baia Mare zone. *Stud. Univ. Babeş-Bolyai Cluj-Napoca Geol.* **1999**, *XLIV*, 151–158.
38. Plotinskaya, O.Y.; Damian, F.; Yu, P.V.; Kovalenker, V.A.; Damian, G. Tellurides occurrences in the Baia Mare region, Romania. *Carpathian J. Earth Environ. Sci.* **2009**, *4*, 89–100.
39. Biruk, S.V.; Skakun, L.Z. Bismuth minerals of the Beregovo ore field: Mineral assemblages and spatial zonation (Transcarpathian, Ukraine). *Geol. Q.* **2000**, *44*, 39–46.
40. Tooth, B.; Brugger, J.; Ciobanu, C.; Liu, W. Modeling of gold scavenging by bismuth melts coexisting with hydrothermal fluids. *Geology* **2008**, *36*, 815–818. [CrossRef]
41. Ciobanu, C.L.; Cook, N.J.; Pring, A.; Brugger, J.; Danyushevsky, L.V.; Shimizu, M. 'Invisible gold' in bismuth chalcogenides. *Geochim. Cosmochim. Acta* **2009**, *73*, 1970–1999. [CrossRef]
42. Seghedi, I.; Downes, H.; Szakács, A.; Mason, P.R.D.; Thirlwall, M.F.; Roşu, E.; Pécskay, Z.; Márton, E.; Panaiotu, C. Neogene-Quaternary magmatism and geodynamics in the Carpathian-Pannonian region: A synthesis. *Lithos* **2004**, *72*, 117–146. [CrossRef]
43. Edelstein, O.; Bernad, A.; Kovacs, M.; Crihan, M.; Pécskay, Z. Preliminary data regarding the K-Ar ages of some eruptive rocks from Baia Mare Neogene volcanic zone. *Rev. Roum. Geol* **1992**, *36*, 45–60.
44. Pécskay, Z.; Edelstein, O.; Kovacs, M.; Bernád, A.; Crihan, M. K/Ar age determination of Neogene volcanic rocks from the Gutâi Mts. (Eastern Carpathians, Romania). *Geol. Carpathica* **1994**, *54*, 357–363.
45. Damian, F.; Damian, G.; Constantina, C. The subvolcanic magmatic rocks from the Nistru zone (Gutii Mountains). *Carpathian J. Earth Environ. Sci.* **2009**, *4*, 101–122.
46. Borcoş, M.; Lang, B.; Peltz, S.; Stan, N. Neogene volcanism evolution in the west part of the Gutâi Mountains (Negreşti-Seini-Băiţa). *Stud. Teh. Econ. Ser. I* **1972**, *6*, 7–36.
47. Sandulescu, M. *Geotectonica Romaniei*, 01. 10. 1984 ed; Editura Tehnica: Bucharest, Romania, 1984; p. 336.
48. Lang, B.; Edelstein, O.; Steinitz, G.; Kovacs, M.; Halga, S. Ar-Ar dating of adularia-a tool in understanding genetic relations between volcanism and mineralization: Baia Mare Area (Gutîi Mountains), Northwestern Romania. *Econ. Geol.* **1994**, *87*, 174–180. [CrossRef]
49. Borisenko, A.S. Study of the salt composition of Fluid Inclusions in Minerals with Cryometric Methods. *Geol. Geofiz.* **1977**, *18*, 16–27.
50. Bodnar, R.J.; Vityk, M.O. Interpretation of microthermometric data for $H_2O$–NaCl fluid inclusions. In *Fluid Inclusions in Minerals: Methods and Applications*; De Vivo, B., Frezzotti, M.L., Eds.; Pontignano: Siena, Italy, 1994; pp. 117–130.
51. Kalyuzhnyi, V.A. Principles of knowledge about mineral forming fluids. *Fluid Incl. Res. Proc. COFFI* **1985**, *15*, 289–333.
52. Brown, P.E. A microcomputer program for the reduction and investigation of fluid inclusion data. *Am. Mineral.* **1989**, *74*, 1390–1393.
53. Kryazhev, S.G.; Prokof'ev, V.Y.; Vasyuta, Y.V. Use of ICP MS Method for Analysis of Composition of Ore-Forming Fluids. *Vestn. Mosk. Univ.* **2006**, *4*, 30–36.
54. Plotinskaya, O.Y.; Damian, G.; Damian, F. Sphalerite assemblages and composition in the Baia Mare region, Eastern Carpathians, Romania (preliminary data). *Rom. J. Miner. Depos.* **2014**, *87*, 87–90.
55. Makovicky, E.; Makovicky, M. Representation of compositions in the bismuthinite-aikinite series. *Can. Mineral.* **1978**, *16*, 405–409.
56. Topa, D.; Makovicky, E.; Balic-Zunic, T. Mineralogical Data on Salzburgite and Paarite, Two New Members of the Bismuthinite Aikinite Series. *Can. Mineral.* **2005**, *43*, 909–917. [CrossRef]
57. Pring, A.; Hyde, B.G. Structural disorder in Lindströmite:A Bismuthinite-Aikinite derivative. *Can. Mineral.* **1987**, *25*, 393–399.
58. Topa, D.; Makovicky, E.; Balic-Zunic, T. The structural role of excess Cu and Pb in gladite and krupkaite based on new refinements of their structure. *Can. Mineral.* **2002**, *40*, 1147–1159. [CrossRef]
59. Topa, D.; Makovicky, E.; Paar, W.H. Composition Ranges and Exsolution Pairs for the Members of the Bismuthinite-Aikinite Series from Felbertal, Austria. *Can. Mineral.* **2002**, *40*, 849–869. [CrossRef]
60. Foord, E.E.; Shawe, D.R.; Conklin, N.M. Coexisting galena, PbSss and sulfosalts: Evidence for multiple episodes of mineralization in the Round Mountain and Manhattan gold district, Nevada. *Can. Mineral.* **1988**, *26*, 355–376.
61. Harris, D.C.; Thorpe, R.I. New observations on matildite. *Can. Mineral.* **1969**, *9*, 655–662.
62. Karup-Møller, S. Mineralogy of some Ag-(Cu)-Pb-Bi sulphide associations. *Bull. Geol. Soc. Den.* **1977**, *26*, 41–68.
63. Moëlo, Y.; Marcoux, E.; Makovicky, E.; Karup-Møller, S.; Legendre, O. Homologues de la lillianite (gustavite, vikingite, heyrovskyite riche en Ag et Bi) de l'indice à W-As-(Pb, Bi, Ag) de la Roche-Balue (Loire-Atlantique, France). *Bull. Minéral.* **1987**, *110*, 43–64. [CrossRef]
64. Topa, D.; Makovicky, E. The Crystal Chemistry of Cosalite Based on New Electron-Microprobe Data and Single-Crystal Determinations of the Structure. *Can. Mineral.* **2010**, *48*, 1081–1107. [CrossRef]
65. Roedder, E. Fluid Inclusions. *Rev. Mineral.* **1984**, *12*, 644. [CrossRef]
66. Wilkinson, J.J. Fluid inclusions in hydrothermal ore deposits. *Lithos* **2001**, *55*, 229–272. [CrossRef]
67. Damian, F.; Cook, N.J. Bi-sulphosalts from the cupriferous mineralisations from Nistru, Baia Mare area. *Rom. J. Mineral.* **1999**, *79*, 27.

68. Baksheev, I.A.; Damian, F.; Damian, G.; Prokofiev, V.Y.; Bryzgalov, I.A.; Marushchenko, L.I. Chemical Composition of Phlogopite, Tourmaline and Illite from Hydrothermal Alterations of the Nistru Deposit, Baia Mare, Romania. *Carpath J. Earth Env.* **2016**, *11*, 547–564.
69. Xu, X.-W.; Zhang, B.-L.; Liang, G.-H.; Qin, K.-Z. Zoning of mineralization in hypogene porphyry copper deposits: Insight from comb microfractures within quartz–chalcopyrite veins in the Hongshan porphyry Cu deposit, western Yunnan, SW China. *J. Asian Earth Sci.* **2012**, *56*, 218–228. [CrossRef]
70. Arehart, G.B.; Chryssoulis, S.L.; Kesler, S.E. Gold and Arsenic in Iron Sulfides from Sediment-Hosted Disseminated Gold Deposits-Implications for Depositional Processes. *Econ. Geol. Bull. Soc.* **1993**, *88*, 171–185. [CrossRef]
71. Reich, M.; Kesler, S.E.; Utsunomiya, S.; Palenik, C.S.; Chryssoulis, S.L.; Ewing, R.C. Solubility of gold in arsenian pyrite. *Geochim. Cosmochim. Acta* **2005**, *69*, 2781–2796. [CrossRef]
72. Marcoux, E.; Molo, Y.; Leistel, J.M. Bismuth and cobalt minerals as indicators of stringer zones to massive sulphide deposits, Iberian Pyrite Belt. *Miner. Depos.* **1996**, *31*, 1–26. [CrossRef]
73. Kovalenker, V.A.; Naumov, V.B.; Prokof'ev, V.Y.; Jelen, S.; Gaber, M. Compositions of Magmatic Melts and Evolution of Mineral-Forming Fluids in the Banska Stiavnica Epithermal Au–Ag–Pb–Zn Deposit, Slovakia: A Study of Inclusions in Minerals. *Geochem. Int.* **2006**, *44*, 118–136. [CrossRef]
74. Beane, R.E.; Bodnar, R.J. Hydrothermal Fluids and Hydrothermal Alteration in Porphyry Copper Deposits. *Porphyry Copp. Depos. Am. Cordill.* **1995**, 83–93.
75. Prokofiev, V.Y.; Kovalenker, V.A.; Jeleň, S.; Borisenko, A.S.; Borovikov, A.A. Determination of Metal Concentrations in Fluid Inclusions Formed during the Magmatic and Hydrothermal Stages of Formation of the Epithermal Au–Ag Polymetallic Deposit of Banska Stiavnica (Western Carpathians) with the LA–ICP–MS Method. *Dokl. Earth Sci.* **2011**, *440*, 1249–1252. [CrossRef]
76. Yue, Q.; Zhai, D.; Zhao, G.; Zhao, Q.; Liu, J. The Occurrence and Chemical Composition of Bismuth-Bearing Minerals in the Niuxingba-Liumukeng Ag-Pb-Zn Deposit, Jiangxi Province, South China. *Minerals* **2024**, *14*, 53. [CrossRef]
77. Shin, D.; Park, H.I.; Lee, I.; Lee, K.S.; Hwang, J. Hydrothermal As–Bi mineralization in the Nakdong deposits, South Korea: Insight from fluid inclusions and stable isotopes. *Can. Mineral.* **2004**, *42*, 1465–1481. [CrossRef]
78. Yunsheng, R.; Liandeng, L.; Huihuang, Z. Gold deposits rich in bismuth minerals: An important type of gold deposits. In Proceedings of the Mineral Deposit Research: Meeting the Global Challenge: Proceedings of the Eighth Biennial SGA Meeting Beijing, Beijing, China, 18–21 August 2005; pp. 581–583.
79. Cioflica:, G.; Jude, R.; Berbeleac, I.; Udubasa, S. Neogene gold mineralization types in Romania. In Proceedings of the XVII Congress of Carpathian-Balkan Geological Association, Bratislava, Romania, 1–4 September 2002.